



Applied machine learning-based models for predicting the geomechanical parameters using logging data

Manouchehr Sanei¹ · Ahmad Ramezanzadeh¹ · Mohammad Reza Delavar¹

Received: 14 November 2022 / Accepted: 27 July 2023 / Published online: 23 August 2023
© The Author(s) 2023

Abstract

Geomechanical (GM) parameters play a significant role in geomechanical studies. The calculation of GM parameters by analyzing finite rock samples is very limited. The GM parameters show a nonlinear trend; thus, applying empirical relationships is unreliable to predict their quantities. Machine learning (ML) methods are generally used to improve the estimation of such parameters. Recent researches show that ML methods can be useful for estimating GM parameters, but it still requires analyzing different datasets, especially complex geological datasets, to emphasize the correctness of these methods. Therefore, the aim of this study is to provide a robust recombinant model of the ML methods, including genetic algorithm (GA)–multilayer perceptron (MLP) and genetic algorithm (GA)–radial basis function (RBF), to estimate GM parameters from a complex dataset. To build ML models, 48,370 data points from six wells in the complicated Norwegian Volve oil field are used to train GA–MLP and GA–RBF methods. Moreover, 20,730 independent data points from another three wells are used to verify the GM parameters. GA–MLP predicts GM parameters with the root-mean-squared error (RMSE) of 0.0032–0.0079 and coefficient determination (R^2) of 0.996–0.999. It shows similar prediction accuracy when used to an unseen dataset. Comparing the results indicates that the GA–MLP model has better accuracy than the GA–RBF model. The results illustrate that both GA–MLP and GA–RBF methods perform better at estimating GM parameters compared to empirical relationships. Concerns about the integrity of the methods are indicated by assessing them on another three wells.

Keywords Geomechanical parameters · Multilayer perceptron · Radial basis function · Well logging · Genetic algorithm

Abbreviations

ANN	Artificial neural network
FL	Fuzzy logic
FN	Functional network
GA	Genetic algorithm
GPM	Gallon per minute
GR	Gamma ray
ML	Machine learning technique
MLP	Multilayer perceptron
MSE	Mean-squared error
NPHI	Thermal neutron porosity
POR	Porosity
RF	Random forest
RHOB	Formation bulk density
ROP	Rate of penetration
RPM	Rotating speed in revolution per minute
Rt	Formation true resistivity

SPP	Standpipe pressure
SVM	Support vector machine
WOB	Weight on bit

List of symbols

b_i	Bias vector
b_k	Bias vector
CC	Correlation coefficient
D	Depth, (m)
DT	Compressional wave slowness, ($\mu\text{s}/\text{ft}$)
DTc	Compressional travel time, ($\mu\text{s}/\text{ft}$)
E_d	Dynamic Young's modulus, (Pa)
E_s	Static Young's modulus, (Pa)
f_k	Function
G	Activation function
h_j	Function
m	Sample number
Max	Maximum value
Min	Minimum value
ml	Multiplier
M_m	Measured quantity
M_p	Predicted quantity

✉ Manouchehr Sanei
manouchehr.sanei@gmail.com

¹ Shahrood University of Technology, Shahrood, Iran

\bar{M}_m	Average of the measured quantity
\bar{M}_p	Average of the predicted quantity
n	Number of neurons
ns	Sample size
P_p	Pore pressure, (Pa)
R^2	Coefficient of determination
RMSE	Root-mean-square error
s	Activation function
SD	Standard deviation
V_p	Compressional and shear wave velocity
V_s	Shear wave velocity
w_{ji}	Weight matrix
w_{jk}	Weight of neuron
w_{kj}	Weight matrix
x	Input data
X	Real number
x_i	Each quantity of data
xo	Original data
$x_{(0,1)}$	Normalized data
y	Output data
Y	Scalar function
y_k	Output of the neuron
μ	Average of x_i
ν_d	Dynamic Poisson ratio
ν_s	Static Poisson ratio
ρ	Density, (kg/m ³)

Introduction

The application of geomechanics in the petroleum industry can lead to significant improvements in the economy and optimized operation. In geomechanical studies, parameters such as elastic properties and rock strength are needed for wellbore stability, wellbore collapse, hydraulic fracturing, and sand production (Gholami et al. 2014).

In general, the GM parameters are calculated using two general methods: laboratory tests and in-well measurements. In the laboratory, the strength and elastic properties are measured on the core using the necessary equipment (Sanei et al. 2013, 2015, 2021a; Sanei and Faramarzi 2014). Furthermore, in-well measurements use wave velocity to compute GM characterization (Tiab and Donaldson 2015; Mavko et al. 2020). The problems of laboratory tests are the unavailability of samples due to the lack of access to appropriate laboratory facilities and the high cost of tests. Therefore, recent attention to in-well measurements have increased more than in the past. The advantages of using dynamic in-well measurement methods are non-destructive, cost-effective in terms of cost and time, as well as cover all wellbore distances (Zhang and Bentley 2005).

Dynamic GM parameters are calculated by applying p-wave velocities computed (Chang et al. 2006; Xu et al. 2016). To reduce several problems during drilling and production related to geomechanics, scientists will require to accurately present the GM parameters. The dynamic parameters, such as Poisson ratio, Young's modulus, shear modulus, and bulk modulus, have been computed using logging data since 1950 by geophysics and geosciences. Then, these parameters can be converted to static parameters (Archer and Rasouli 2012; Najibi et al. 2015).

There are many researchers who have developed several predictive and empirical models to estimate GM parameters. These models are based on physical, petrophysical, and index parameters (Sachpazis 1990; Ulusay et al. 1994; Jamshidi et al. 2013; Aladejare 2016, 2020). Empirical relationships can estimate the parameters from well-logging data such as p-wave velocity, s-wave velocity, compressional transient time, shear transient time, density, and porosity (Chang et al. 2006). In addition to these models, drilling data, such as penetration rate (POR) and rotation per minute (RPM), were used to forecast rock strength parameters (Rampersad et al. 1994; Hareland and Nygård 2007). Tables 2 and 3 list some of the most generally used empirical relationships presented for estimating Young modulus, unconfined compressive strength, and Poisson ratio.

In the last few years, machine learning methods have started to use for several purposes. Machine learning includes artificial neural networks (ANNs), radial basis function (RBF), support vector machines (SVMs), random forest (RF), genetic algorithm (GA), etc., which can perform accurately (Mohaghegh 2000). Machine learning is widely used in different issues such as medicine, education, economics, transportation, and more (Elsafi 2014). In the petroleum industry, several machine learning methods have been used to predict different properties with high accuracy compared to other methods (Doraisamy et al. 1998). For instance, history matching process (Costa et al. 2014), pore pressure estimation (Aliouane et al. 2015; Rashidi and Asadi 2018), wellbore stability (Okpo et al. 2016), well planning (Fatehi and Asadi 2017), predicting the in situ stresses (Abusurra 2017; Ibrahim et al. 2021), fracture pressure prediction (Ahmed et al. 2019), reservoir fluids properties estimation (Elkatatny and Mahmoud 2018), permeability prediction (Gu et al. 2018), oil recovery factor estimation (Mahmoud et al. 2019a), predicting the water saturation (Tariq et al. 2019), forecasts oil rate prediction (Kubota and Reinert 2019), prediction of relative permeability (Zhao et al. 2020), predicting permeability impairment (Ahmadi and Chen 2020), prediction of fracture density (Rajabi et al. 2021), fault diagnosis (Jin et al. 2022), predicting movable fluid (Gong et al. 2023), and optimization of drilling parameters (Delavar et al. 2023).

In addition, several researchers have used machine learning to estimate GM parameters. For example, Tariq et al. (2017a) proposed a method to predict failure parameters using ANNs. Naeini et al. (2019) estimated pore pressure and geomechanical properties by considering an integrated deep learning solution. Elkatatny et al. (2019) proposed a scheme to estimate Young's modulus by using machine learning methods. Mahmoud et al. (2019b, 2020) used the machine learning methods to evaluate the Young's modulus. He et al. (2019) estimated the rock strength parameters by applying machine learning methods. Gowida et al. (2020) estimated the unconfined compressive strength by considering machine learning methods based on drilling data. Khatibi and Aghajanjpour (2020) applied machine learning to estimate in situ stresses and GM parameters from offshore gas reservoir information. Ahmed et al. (2021) estimated the Poisson ratio by applying machine learning methods using drilling parameters. Aghakhani Emamqeyasi et al. (2023) predicted the elastic parameters in gas reservoirs using the ensemble method.

It is the fact that most empirical relationships for prediction GM parameters (Tables 2 and 3) limit their accuracy and use them in a specific field. The results of such GM relationships are considerably affected by lithology type, which may present inadequate prediction accuracy (Güllü and Jaf 2016). In addition, the lack of generality of the mentioned methods to other field data and their poor fit limit their reliability (Güllü and Pala 2014). In recent years, the

computational efficiency and predictive accuracy of GM parameters have increased by using a variety of ML methods (Wang et al. 2021). The data applied in these methods are generally verified using a few core measurement data. Table 1 presents some recent researches for calculating GM parameters using ML methods. Although such ML methods in Table 1 improve prediction and also extensive datasets are available worldwide, there are still many goals to improve the prediction accuracy of GM parameters. In addition, there are insufficient researches to present the appropriate feature selected to provide a correct estimation of GM properties, such as Poisson ratio, Young's modulus, and unconfined compressive strength.

The aim of this study is to provide a robust and user-friendly ML model to compute GM parameters from the complex dataset of the Volve field with various anisotropic reservoir rocks. The model can be used to obtain the GM parameters in offset wells without geomechanical measurements in the laboratory from standard well logs. The ML methods include two techniques: MLP and RBF, which are coupled with genetic algorithm (GA). The main novelty and features of this research are to develop, apply, and compare the predicted GM parameters from GA–MLP and GA–RBF methods applied to a very large multiple-well dataset from a complicated Volve oil field which include six wells. The process is done by introducing a suitable feature spectrum to present appropriate GM parameters. The feature spectrum is introduced from the well log data, which are compressional

Table 1 ML methods previously presented for predicting GM parameters

References	Type of GM parameters	Data points	Input parameters	ML techniques	R2
Abdulraheem et al. (2009)	Static Young's modulus	77	V_p, V_s, ρ	ANN, FL, FN	0.593–0.792
Al-anazi et al. (2011)	Static Young's modulus	602	$V_p, V_s, \rho, D_{th}, POR, P_p$	ACE	0.974
Tariq et al. (2017b)	Static Young's modulus	550	V_p, V_s	ANN	0.92
Elkatatny et al. (2019)	Static Young's modulus	600	V_p, V_s, ρ	ANN, ANFIS, SVM	0.87–0.92
Mahmoud et al. (2019b)	Static Young's modulus	592	V_p, V_s, ρ	ANN	0.998
Mahmoud et al. (2020)	Static Young's modulus	630	RHOB, DTc, DTs	ANN, M-FIS, FNN, SVM	0.998
Siddig and Elkatany (2021)	Static Young's modulus	2288	WOB, Tor, SPP, RPM, ROP, FR	ANN, SVM	0.88–0.98
Hassanvand et al. (2018)	Uniaxial compressive strength	121	POR, ρ, S_w	MLP, RBF	0.83
Gowida et al. (2020)	Uniaxial compressive strength	2175	WOB, Tor, SPP, RPM, ROP, GPM	ANN, ANFIS, SVM	0.98
Asadi (2017)	Uniaxial compressive strength	77	DTc, POR, ROP, ρ	ANN	0.99–1
Nabaei and Shahbazian (2012)	Uniaxial compressive strength	30,000	DTc, POR	ANN	0.96
Siddig et al. (2021)	Poisson ratio	2912	WOB, Tor, SPP, RPM, ROP, GPM	ANN, ANFIS	0.97–0.98
Asoodeh (2013)	Poisson ratio	1582	DTc, NPHI, Rt, RHOB	FL	0.82
Ahmed et al. (2021)	Poisson ratio	762	WOB, Tor, SPP, RPM, ROP, Q	FN, RF	0.94

wave transmission time (DT), lithology index (LI), density (RHOB), coordinate X, coordinate Y, coordinate Z, measurement depth (MD), shear wave transmission time (DTs), and neutron porosity (NPHI). The predicted GM parameters' performance of GA–MLP and GA–RBF methods is also compared, for the same dataset, with generally used empirical predicted GM parameter models. This process identifies the most effective model for predicting the GM parameters. To verify the results, we address possible concerns about ensuring the integrity of the proposed ML models by applying them to the other data from three wells in the oil field. Although this method is known as a fast and low-cost solution compared to the other existing methods, this technique has some disadvantages. For example, hardware and software limitations (appropriate computer system for processing power) and sometimes the lack of access to high-quality data from the well lead to errors in the prediction of GM parameters. However, in general, the advantages of the ML methods are more than their disadvantages and can be widely used in the industry with the development of suitable computational platforms.

Methodology

Multilayer perceptron

Artificial neural network (ANN) is a type of machine learning method used for various problems (Ali 1994). Multilayer perceptron (MLP) is one of the subsets of ANN model that acts as a global approximator (Hornik 1991). MLP has three layers, namely input, output, and hidden, as indicated in Fig. 1. The input layer is the layer that receives the signal

for processing. Tasks such as classification and prediction are done based on the output layer. MLP includes one or several hidden layers. Each node in the output and hidden layers is a neuron that considers an activation function. The difference between the output and target is the residual error (Wei et al. 2021).

As presented in Fig. 1, the input layer includes a set of neurons $\{x_i | x_1, x_2, \dots, x_i\}$. Each neuron in the hidden layer transforms the values from the previous layer and followed by a nonlinear activation function $g(\cdot) : R \rightarrow R$ like the hyperbolic tan function. The computations are as follows (Menzies et al. 2014):

$$h_j = s(w_{ji}x_i + b_i) \quad (1)$$

$$f_k = G(w_{kj}h_j + b_k) \quad (2)$$

where b_i, b_k are the bias vectors, w_{ji}, w_{kj} are the weight matrices, and G and s are the activation functions.

Radial basis function (RBF)

Radial basis function (RBF) network is combined of three layers such as input, hidden, and output (Haykin 1999; Yu and He 2006). The first layer is the inputs of the network, the second is a hidden layer including a number of RBF functions, and the last one is the output. RBF includes just one hidden layer. Figure 2 indicates an example of the RBF structure.

The input is modeled by a vector of real numbers $X \in R^n$. The output is a scalar function of the input, $Y : R^n \rightarrow R$, and is presented by:

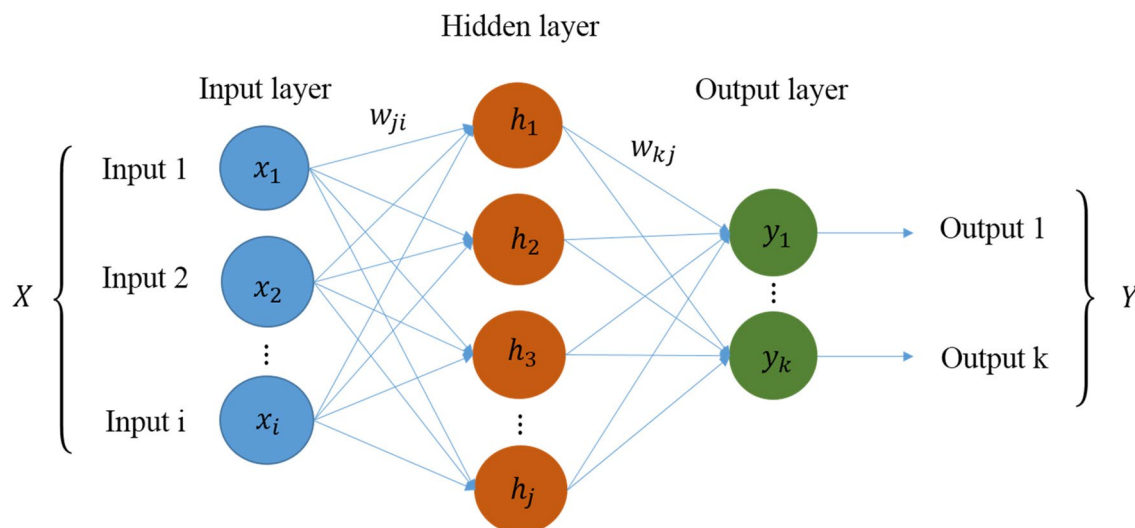


Fig. 1 Schematic representation of the MLP with a single hidden layer

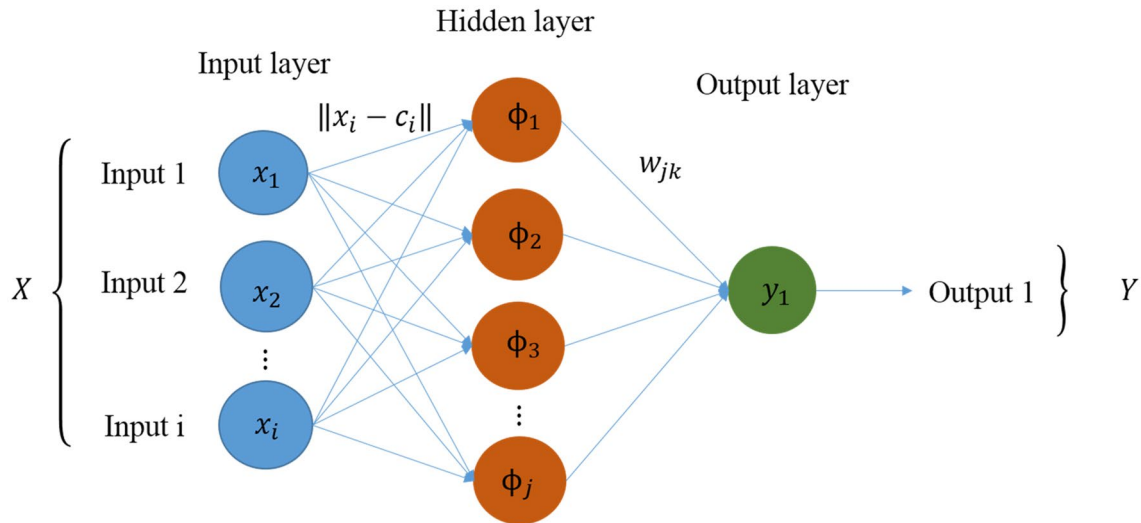


Fig. 2 Example of RBF network

$$y_k = \sum_{j=1}^n w_{jk} \phi_j \tag{3}$$

where n is the number of neurons, w_{jk} is the weight of neuron j , and y_k is the output of the neuron k .

Genetic algorithm

The genetic algorithm (GA) is a metaheuristic algorithm proposed by Holland (1992). This method is applied to solving constrained and unconstrained optimization problems based on the natural selection process, which mimics biological evolution. The algorithm iteratively changes the population of individual solutions. At each step, the genetic algorithm randomly chooses individuals from the current population and uses them as parents to produce offspring for the next generation.

GA starts with an initial population of randomly generated chromosomes, where each chromosome represents a possible solution to the given problem. Each chromosome is associated with a fitness value, which is a measure of how good a solution is to the given problem. In each generation, the population evolves toward better fitness using evolutionary operators such as selection, crossover, and mutation. This process continues until a solution is found or the maximum number of iterations is reached. Figure 3 shows the GA process in a flowchart.

GA-MLP algorithm

In order to improve the accuracy of the MLP method, it is essential to optimize the value of parameters that should be

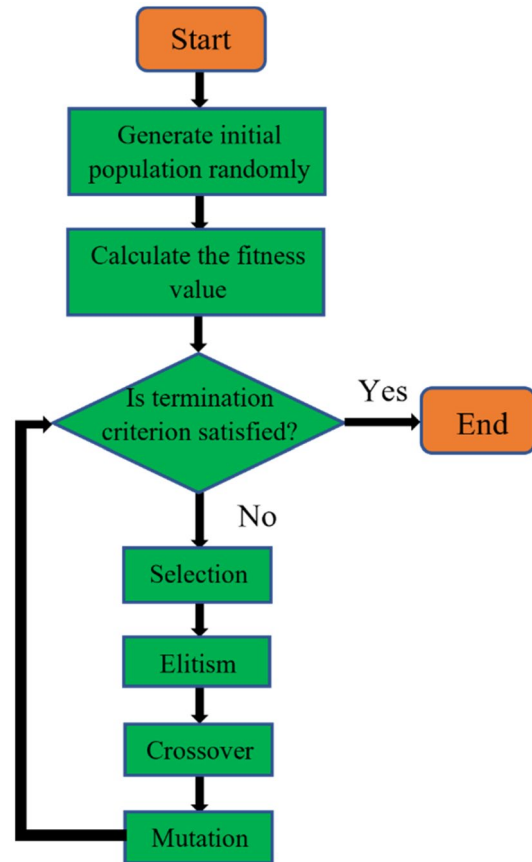


Fig. 3 Flowchart of the execution sequence of a GA

determined during the design of the MLP method. These parameters are weights and biases. Various algorithms have been proposed to present the quantities of weights and

biases. Some researchers have suggested the genetic algorithm (GA) approach to generate an optimal set of weights and biases for the multilayer perceptron (MLP) method (Bansal et al. 2022). Therefore, in this study, the GA–MLP algorithm is applied to the subsequent sections. This algorithm improves the performance of the MLP by using a GA approach to generate the initial values of each parameter. Figure 4 (left) shows the workflow of the GA–MLP algorithm.

GA–RBF algorithm

In order to improve the accuracy of the RBF method, it is essential to optimize the value of parameters such as weights and biases. A variety of algorithms have been developed to propose the quantities of weights and biases. As the same above section, genetic algorithm (GA) can generate an optimal quantity of weights and biases for the RBF model (Jia et al. 2014). Therefore, in this study, the GA–RBF algorithm is applied to the next sections. This algorithm improves the performance of the RBF method. Figure 4 (right) shows the workflow of the GA–RBF algorithm.

Case study

Regional background

This paper is performed based on the Volve information, Norway, as indicated in Fig. 5. The structure of reservoir is a small dome shape (Equinor Website Database 2021; Szydlik et al. 2006). The reservoir formation belongs to Hugin and produced from sandstone.

In this study, the information of nine wells is selected, which has been released by the Equinor company (Equinor Website Database 2021).

Geology of the region

In this field, the reservoir part is the Hugin formation and the caprock is the Heather and Draupne formations. The rocks generally are sandstone, siltstone, claystone, limestone, marl, calcite, tuff, and coal as illustrated in Fig. 6. The Volve field is geologically complicated as illustrated in Fig. 7.

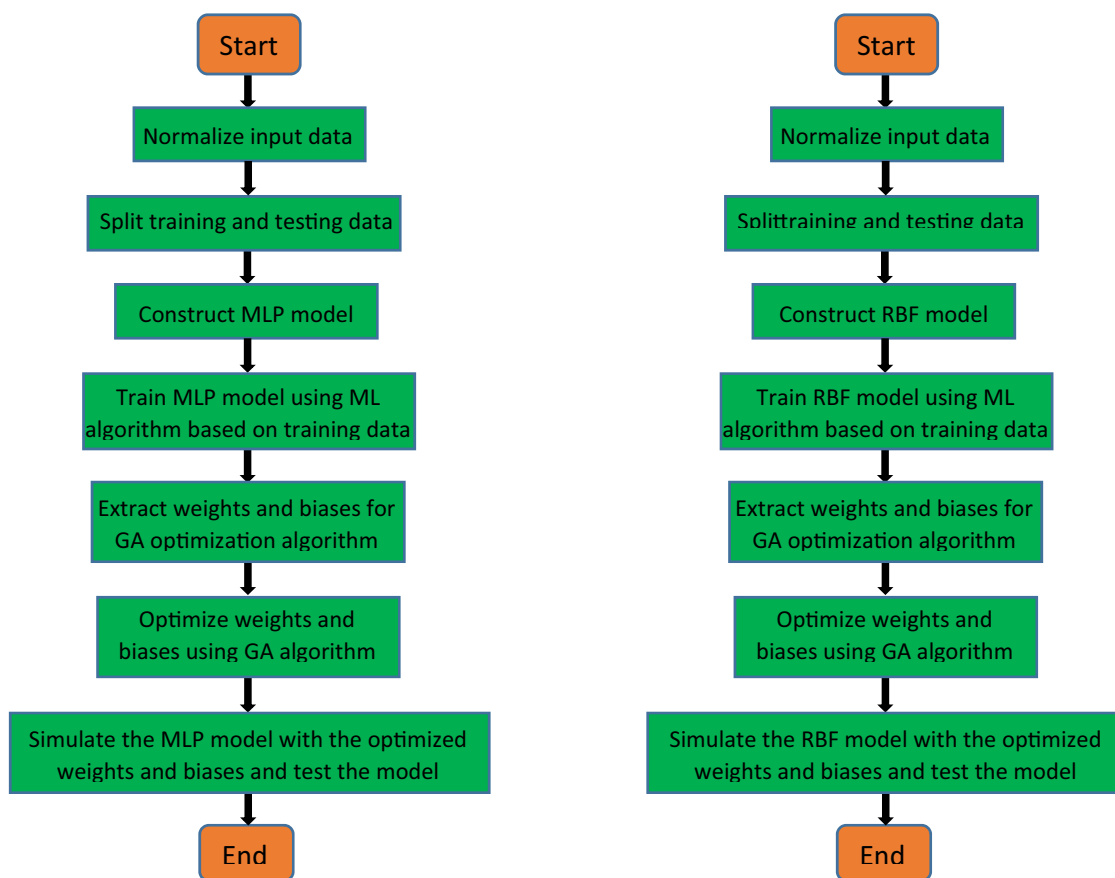


Fig. 4 The workflow of: (left) GA–MLP, (right) GA–RBF algorithm

Fig. 5 The location of the Volve field (Sen and Ganguli 2019)

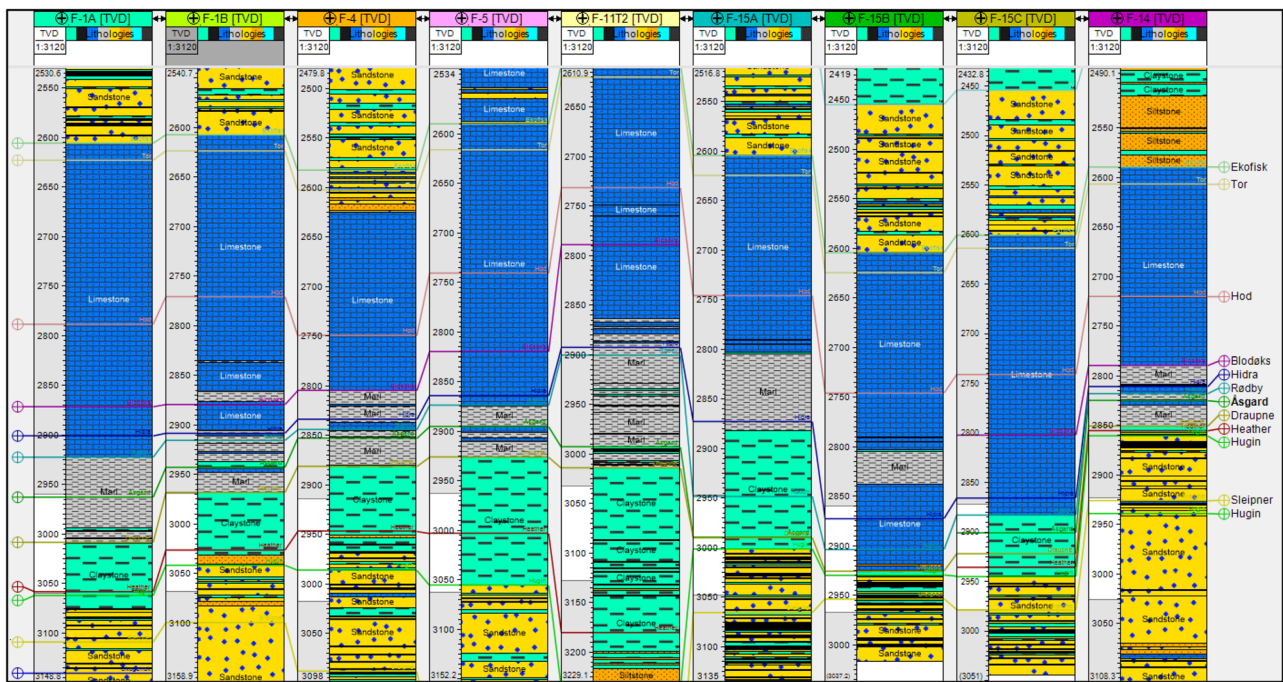
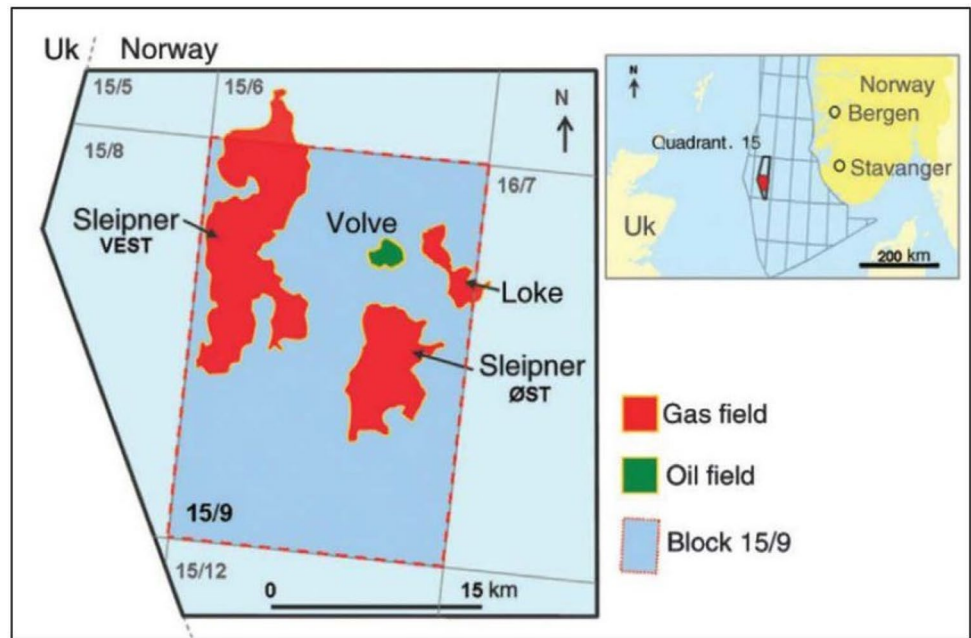


Fig. 6 Stratigraphic column of the Volve field, Norway

Estimation of geomechanical (GM) properties

There are many methods in the petroleum industry to measure or estimate GM properties, such as elastic properties and rock strength. Correct estimates help to have appropriate knowledge of the various problems (Zhang

2020; Sanei et al. 2021b, 2022). The methods for direct measurement of geomechanical properties commonly are expensive and limited. The empirical models presented for estimating the geomechanical properties based on the well log data can provide the correct value if the parameters of models are computed appropriately.

As we want to present the continuous profile of parameters along with each well, geomechanical properties

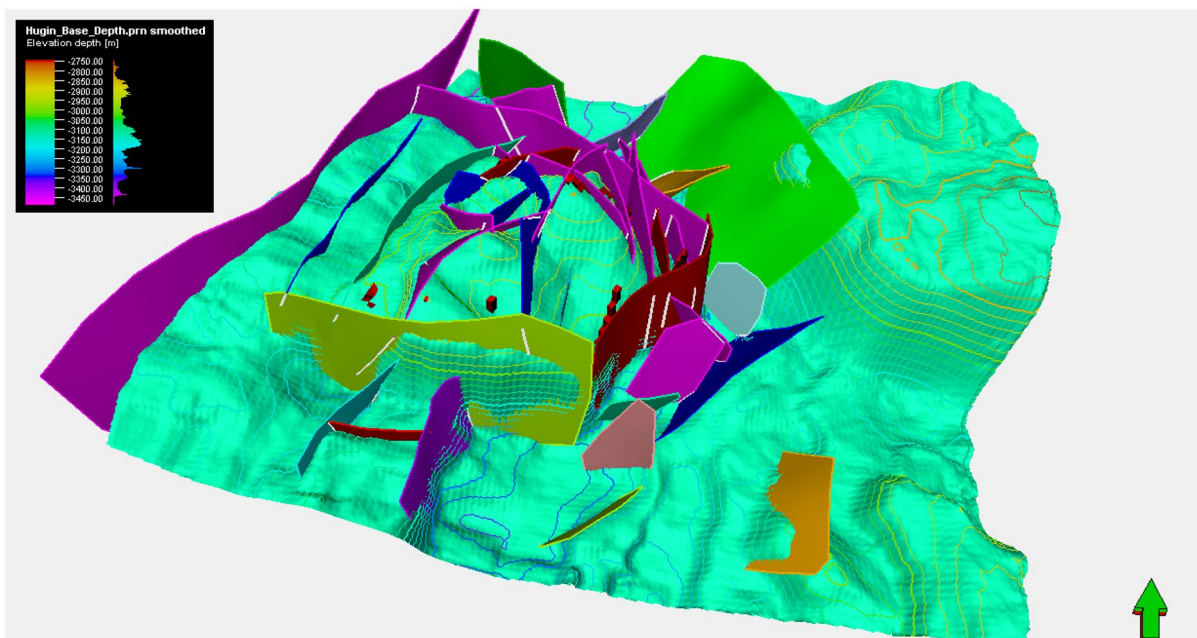


Fig. 7 Three-dimensional view of the Volve field

Table 2 Models to estimate static Young’s modulus

Models	Equations	Description
John Fuller, Schlumberger (2018)	$E_s = 0.032 \times (E_d)^{1.632}$	The UCS quantity is mainly between 2000 and 10,000 psi
Plumb Bradford, Schlumberger (2018)	$E_s = 0.0018 \times (E_d)^{2.7}$	It is for sandstone. The average porosity is 22%, and the average permeability is 70 mD
Sandstone-Morales, Schlumberger (2018)	$\log(E_s) = 2.137 + 0.6612 * \log(E_d)$	Porosity 10–15%
	$\log(E_s) = 2.137 + 0.6612 * \log(E_d)$	Porosity 15–25%
	$\log(E_s) = 2.137 + 0.6612 * \log(E_d)$	Porosity > 25%
Modified Morales, Schlumberger (2018)	$E_s = (-2.21 \phi + 0.965)E_d$	It is for sandstone. ϕ is the porosity (ϕ if $\phi \leq 0.35$ and $\phi = 0.35$ if $\phi > 0.35$)
Morals, Wang (2000)	$E_s = 0.4145E_d - 1.0593$	
Lacy (1997)	$E_s = 0.018E_d^2 + 0.422E_d$	It is for sandstone, shale, siltstone, and dolomite
Lacy (1997)	$E_s = 0.265E_d^{2.04}$	It is for sandstone, shale, siltstone, and dolomite

such as Young’s modulus, uniaxial compressive strength (UCS), and Poisson ratio for training and testing the machine learning model are essential. They can be synthetically generated through the empirical relationships, as the continuous data are not measured along the wall and is limited to some points. Although the machine learning methods to predict such variables are proven using synthetic data, the scheme can also be performed with real data of Young’s modulus, uniaxial compressive strength (UCS), and Poisson ratio, if available.

Elastic properties

The elastic parameters are computed from two methods, namely laboratory measurement based on core samples (static method) and determination of elastic constants using the well log data (dynamic method). The results show that the values obtained from dynamic methods are larger than static methods (Plona and Cook 1995).

Dynamic elastic properties

The dynamic Young's modulus E_d [GPa] and dynamic Poisson ratio ν_d [%] are calculated as: (Fjær et al. 2008):

$$E_d = \rho V_s^2 \frac{3V_p^2 - 4V_s^2}{V_p^2 - V_s^2} \quad (4)$$

$$\nu_d = \frac{V_p^2 - 2V_s^2}{2(V_p^2 - V_s^2)} \quad (5)$$

where ρ is the bulk density (g/cm^3), V_p is the compressional velocity [km/s], and V_s is the shear velocity [km/s].

Static elastic properties

To estimate the static parameters from dynamic parameters, many equations have been presented. The well-known equations to estimate static Young's modulus are presented in Table 2.

The static Poisson ratio ν_s is calculated from dynamic Poisson ratio ν_d as follows:

$$\nu_s = ml \times \nu_d \quad (6)$$

where ml is the multiplier. Some researchers, including Archer and Rasouli (2012), believed that the $ml = 1$. However, Afsari et al. (2009) expressed that the $ml = 0.7$.

Static Young's modulus and Poisson ratio can be estimated using different equations as expressed above based on logging data. In this manner, different models are used and compared with each other to know which model is the best for estimating the synthetical data of static Young's modulus and Poisson ratio. The process has been done, and the results show that the John Fuller model has a good ability to estimate the static Young's modulus. In addition, the static Poisson ratio shows that the best multiplier is $ml = 1$. The process to estimate static Young's modulus and the static Poisson ratio is performed based on the data of well F1A. The results in Fig. 8 indicate that the mentioned models can estimate parameters precisely. The same procedure for well F1A as shown in Fig. 8 is performed for other wells.

Rock strength

Unconfined compressive strength (UCS) can be calculated in two ways, one based on uniaxial compression tests on drilling cores, and the other one is obtained by using several empirical relationships based on well-log data. Some well-known relationships are presented in Table 3.

Unconfined compressive strength can be obtained from logging data using various equations as expressed above. In this manner, different models are used and compared with each other to know which model is the best for estimating the synthetical data of unconfined compressive strength. The process is carried out, and the results show that the Dick Plumb model has a good capability to correctly estimate the unconfined compressive strength, as presented, for well F1A in Fig. 8. The same procedure for well F1A is performed for other wells to produce the continuous profile unconfined compressive strength.

Development of neural networks

Normalization method

Data normalization is one of the basic requirements for machine learning (Anysz et al. 2016). Input data generally have different units and dimensions. Normalization causes the model to converge quickly and minimizes error (Rojas 1996). Here, min–max normalization method (as given in Eq. 7) is used to normalize the data in the range of zero to one.

$$x_{(0,1)} = \frac{x_o - \text{Min}}{\text{Max} - \text{Min}} \quad (7)$$

where x_o and $x_{(0,1)}$ are the original and normalized data, respectively; Min and Max represent the minimum and maximum values of the whole dataset.

Statistical criteria

The performance of machine learning can be analyzed. Several important criteria are considered to assess the efficiency and accuracy of these models. The criteria are the coefficient of determination (R^2), root-mean-square error (RMSE), and a standard deviation (SD), which can evaluate the overall performance of the model. Equations 8–10 are applied to calculate these parameters.

$$R^2 = \frac{(\sum_{i=1}^n (M_m - \bar{M}_m)(M_p - \bar{M}_p))^2}{\sum_{i=1}^n (M_m - \bar{M}_m)^2 \sum_{i=1}^n (M_p - \bar{M}_p)^2} \quad (8)$$

$$\text{RMSE} = \sqrt{\frac{\sum_{i=1}^n (M_p - \bar{M}_m)^2}{n}} \quad (9)$$

$$\text{SD} = \sqrt{\frac{\sum_{i=1}^n (x_i - \mu)^2}{m - 1}} \quad (10)$$

where M_m and M_p are the measured and predicted quantities, respectively, \bar{M}_m and \bar{M}_p are the average of the measured and

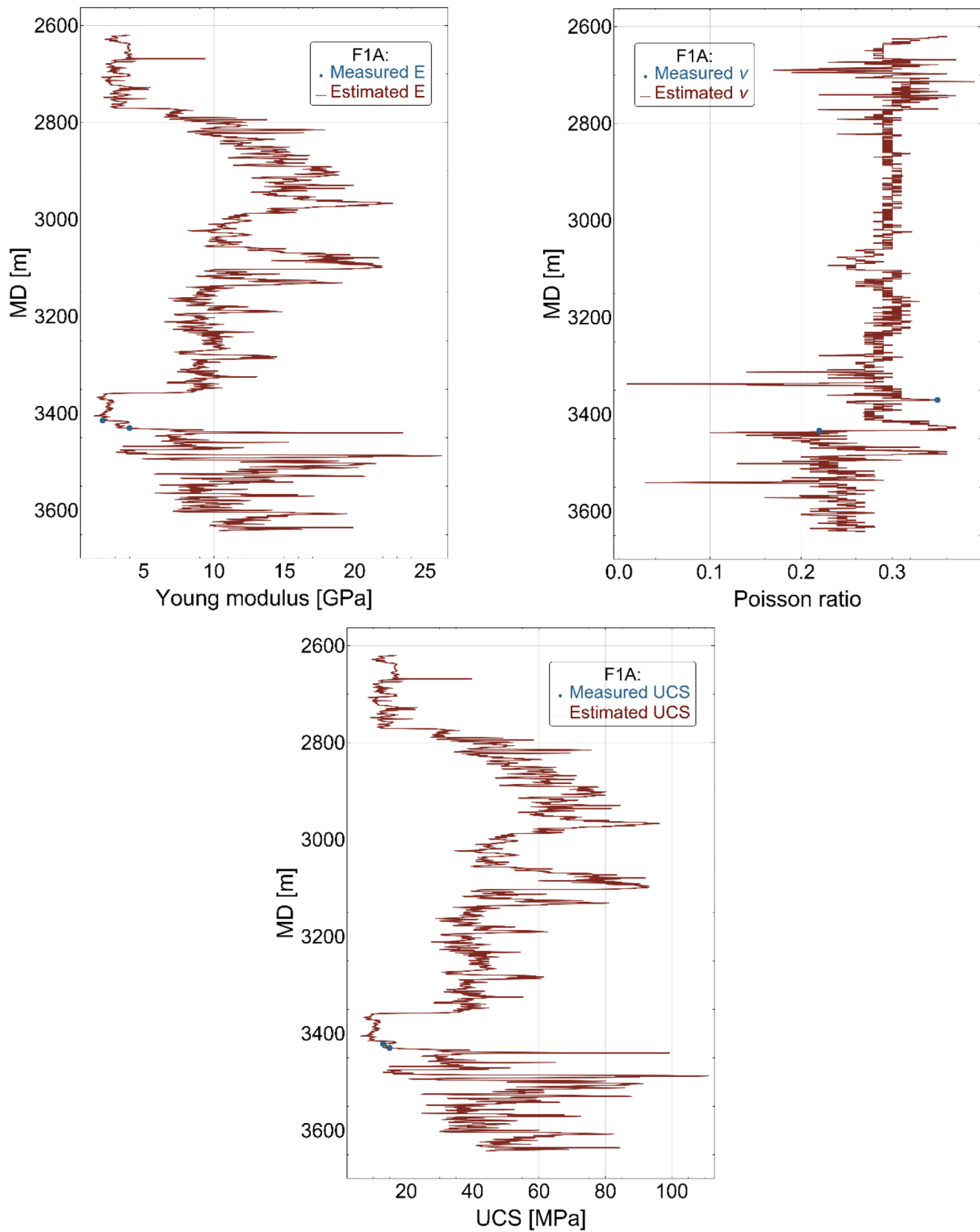


Fig. 8 Comparison of: (top-left) measured static Young's modulus with John Fuller model results, (top-right) measured and estimated Poisson ratio with multiplier, $m = 1$, (bottom) measured unconfined compressive strength with Dick Plumb model results for well F1A

predicted quantities, respectively, m represents the sample number, x_i is each quantity of data, and μ is an average of

x_i . According to previous studies, the systems can present to good performance when they have a high coefficient of

Table 3 Models for estimating the unconfined compressive strength

Models	Equations	Description
Dick Plumb, Schlumberger (2018)	$UCS = 4.242 \times E_s$	It is for sandstones and shales
Plumb porosity, Schlumberger (2018)	$UCS = 437(1 - 2.22\phi)^{3.6756}$	The UCS sets as 145 psi for porosity, $\phi > 0.365$
Brie shear modulus, Schlumberger (2018)	$UCS = 5.6 \times 10^{-6} G_{ref,sand} \left(\frac{G_{dyn}}{G_{ref,sand}} \right)$	It is for sandstones. G_{dyn} is the dynamic shear modulus
	$UCS = 12.0 \times 10^{-6} G_{ref,sand} \left(\frac{G_{dyn}}{G_{ref,sand}} \right)$	It is for shales
McNally, Schlumberger (2018)	$UCS = 1200 \exp^{-0.036 \times DT}$	DT is the compressional slowness. It is valid for sandstones
Plumb shear modulus, Schlumberger (2018)	$UCS = 0.12(G_{dyn})^{2.3}$	It is for sand, sandstones, and siltstones with porosity $0 \leq \phi \leq 0.4$
Zoback (2010)	$UCS = 1200 \exp(-0.036DT)$	It is for sandstones
Zoback (2010)	$UCS = 1.4138 \times 10^7 DT^{-3}$	It is for sandstones
Plumb Young’s MODULUS, Bradford et al. (1998)	$UCS = 2.280 + 4.1089 \times E_s$	It is for sandstones and shales
Plumb porosity correlation, Schlumberger (2018)	$UCS = 243(1 - 2.857\phi)^2$	It is for sandstones
	$UCS = 70(1 - 2.222\phi)^2$	It is for shales
Fjær et al. (2008)	$UCS = 357(1 - 2.8\phi)^2$	It is valid for sandstone. With porosity, $\phi < 0.357$
Fjær et al. (2008)	$UCS = 193\phi^{-1.14}$	It is for shales
Horsrud, Schlumberger (2018)	$UCS = 0.77 \left(\frac{304.8}{DT} \right)^{2.93}$	It is for shales

determination (close to 1) and a low error value of RMSE (close to zero) (Ranjbar-Karami et al. 2014; Armaghani et al. 2015; Elkatatny et al. 2019).

Data processing and analysis

Data processing

Machine learning models are data-driven, and inserting all available parameters to serve as an input does not always guarantee good results. The best practice is to find which input parameter is contributing positively and which input contributes negatively. A multivariate linear regression correlation coefficient feature selection system is used to estimate the individual relationship in terms of the correlation coefficient between input and output parameters as illustrated in Fig. 9. The correlation coefficient (CC) between input and output can be calculated by Eq. (11) (Elkatatny et al. 2019).

In machine learning models, applying all available parameters as input to the model usually does not guarantee good results. One of the best methods is to choose which input parameters have a positive effect and which have a negative effect on the results. Accordingly, a feature selection system such as correlation coefficient between input and output parameters can be used as shown in Fig. 9. The correlation coefficient (CC) is:

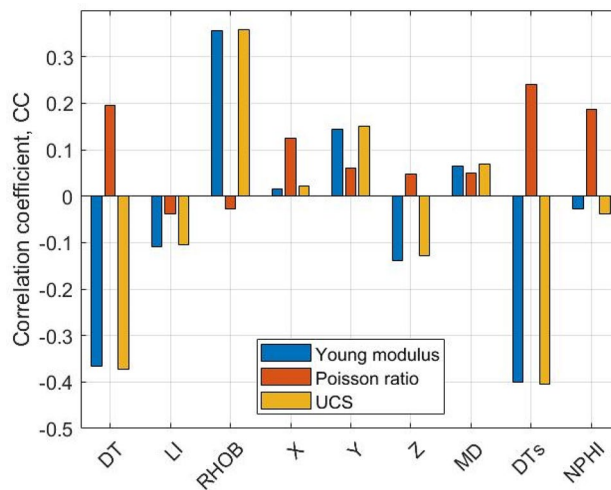


Fig. 9 Correlation coefficient between input data with Poisson ratio, Young’s modulus, and UCS

$$CC = \frac{ns \sum xy - (\sum x)(\sum y)}{\sqrt{ns(\sum x^2) - (\sum x)^2} \sqrt{ns(\sum y^2) - (\sum y)^2}} \quad (11)$$

where ns is the sample size, x and y are the input and output data. In order to analyze the input parameters in this study, the correlation coefficient as obtained by Eq. (11) between the available data, such as (DT, LI, RHOB, X, Y, Z, MD, DTs, NPHI) as input data, and the values of Poisson ratio,

Young's modulus, and UCS as output data are calculated. The results of the correlation coefficient presented in Fig. 9 show that Young's modulus and UCS have an inverse relationship with DT, LI, Z, DTs, and NPHI and a direct relationship with RHOB, X, Y, and MD. In addition, the results present that the Poisson ratio parameter has an inverse relationship with LI and RHOB and a direct relationship with other input parameters, namely DT, X, Y, Z, MD, DTs, and NPHI.

Data description

Data preparation is one of the necessary steps to be a success in machine learning algorithms. The performance of models depends on having high-quality information. In this research, according to the correlation coefficient results (Fig. 9), a suitable feature spectrum is introduced as input parameters, such as compressional wave transmission time (DT), lithology index (LI), density (RHOB), coordinate X, coordinate Y, coordinate Z, measurement depth (MD), shear wave transmission time (DTs), and neutron porosity (NPHI)

to provide appropriate geomechanical parameters. In this research, information of nine wells, i.e., a total of 69,100 data, is used, which are the result of well logging. The data include different formations, different wells, and different depths. The machine learning models will be implemented in two modes. In whole modes, the input data are divided into three categories: 70% data as train data, 15% as test data, and 15% as validation data. The data for the statistical analysis before normalizing are given in Table 4 and after normalizing are presented in Table 5.

Building a GA-MLP algorithm configurations

The performance of the MLP model is dependent on the number of hidden layers and the number of neurons. The more the complex problem, the greater the number of hidden layers and neurons, which causes a longer computational time. Then, optimizing the MLP structure can increase the performance and accuracy of this model. A trial-and-error learning method can be a suitable method to calculate the number of hidden layers (Ham and Kostanic 2001), but this

Table 4 Data for the statistical analysis before normalizing

Parameters	Max	Min	Mean	Range	SD	Skewness	Kurtosis
DT	136.25	48.28	77.0215	87.97	13.29302	0.951922	0.81208
LI	6	0	2.361635	6	1.396792	-0.17747	-0.53989
RHOB	3.2013	1.0988	2.45524	2.1025	0.162554	-1.18985	2.13716
X	436,395.7	433,822.2	435,279.4	2573.52	590.0807	-0.1584	-0.4812
Y	6,479,427	6,477,700	6,478,666	1726.721	532.2401	-0.42452	-1.22841
Z	3306.961	2390.109	2807.213	916.8522	185.8399	0.144736	-0.47922
MD	4522.3	2575.9	3308.431	1946.4	417.9216	0.765927	0.242895
DTs	388.84	84.48	144.6985	304.36	33.50887	1.839739	4.060598
NPHI	0.5	0	0.130347	0.5	0.069678	1.10679	1.2343
E	37.74338	0.135211	9.249372	37.60817	4.031083	0.696373	1.285333
ν	0.452336	0.001532	0.267442	0.450804	0.054774	-1.05989	2.848713
UCS	160.1018	0.698594	39.06799	159.4032	17.03306	0.728086	1.382594

Table 5 Data for the statistical analysis after normalizing

Parameters	Max	Min	Mean	Range	SD	Skewness	Kurtosis
DT	1	0	0.326719	1	0.151109	0.951922	0.81208
LI	1	0	0.393606	1	0.232799	-0.17747	-0.53989
RHOB	1	0	0.645156	1	0.077315	-1.18985	2.13716
X	1	-9.3E-09	0.566237	1	0.229289	-0.1584	-0.4812
Y	0.999969	1.95E-07	0.559411	0.999969	0.308228	-0.42452	-1.22841
Z	1	4.56E-10	0.454931	1	0.202693	0.144736	-0.47922
MD	1	0	0.376352	1	0.214715	0.765927	0.242895
DTs	1	0	0.197853	1	0.110096	1.839739	4.060598
NPHI	1	0	0.260695	1	0.139357	1.10679	1.2343
E	1	0	0.242345	1	0.107186	0.696373	1.285333
ν	1	0	0.589858	1	0.121503	-1.05989	2.848713
UCS	1	0	0.240707	1	0.106855	0.728086	1.382594

Table 6 Control parameter values for the GA–MLP algorithm

MLP		GA	
Control parameter	Value/options	Control parameter	Value/options
Number of inputs	9	Population	60
Number of hidden layers	1	Selection method	Roulette wheel
Number of input layer neurons	40	Crossover	Uniform, ($p = 1$)
Number of output layer neurons	1	Mutation	Uniform, ($p = 0.05$)
		Mutation rate	0.11
		Selection pressure for roulette wheel	2

is a time-consuming method. Therefore, in this study, the GA algorithm is used to calculate the number of MLP hidden layers and the number of neurons in each layer. A schematic of how to implement the GA–MLP model is shown in Fig. 4(left). Table 6 indicates the control parameter values of the GA–MLP algorithm, which are essential for optimizing the number of layers and neurons.

In the MLP, the neurons are connected in the neural network through feed-forward type. The sigmoid tangent transfer function is applied to the hidden layer, and the linear function is applied to the output layer. The Levenberg–Marquardt algorithm is applied to train the network. Figure 10 shows a schematic of the different steps of MLP model.

Building a GA–RBF algorithm configurations

The radial basis function (RBF) network has a simple structure and a fast-training process (Wu et al. 2012). Choosing a sufficient number of neurons for the one hidden layer in RBF is required to satisfy the specific mean-squared error. The optimization of the RBF structure can increase the performance and accuracy of this method. Therefore, in this study, the GA algorithm is applied to determine the number of spreads and neurons in the RBF method. A schematic of how to implement the GA–RBF model is illustrated in Fig. 4(right). Table 7 indicates the control parameter values of the GA–RBF algorithm which are essential for optimizing the number of spreads and neurons.

In the RBF, activation functions in RBF are performed using Gaussian functions. The radial basis function is applied to the hidden layer, and the linear function is applied to the output layer. Figure 11 illustrates a schematic of the different steps of the RBF model.

Results and discussion

In this study, to provide a robust ML model to compute GM parameters from the complex dataset, which can be used to obtain the GM parameters in offset wells without geomechanical measurements in the laboratory, the datasets of the

nine wells of the Volve oil field are used. The appropriate ML model for geomechanical properties is selected based on two data sets. First, the datasets of five wells, namely F1A, F1B, F4, F5, and F11T2, and second, all data of nine wells, in which the data records split 70%:30% between training and validation subsets. The two sets of datasets are given separately to ML methods to predict the GM properties, such as Young's modulus, UCS, and Poisson ratio and compared the results with measured data.

Prediction of geomechanical properties for some wells

In this section, to present the capability of GA–MLP and GA–RBF models to predict geomechanical parameters such as the static Poisson ratio, Young's modulus, and UCS, the data set of wells number F1A, F1B, F4, F5, F11T2 is used and named as F1–F11. The mentioned machine learning methods for each geomechanical property are built based on nine input data, namely DT, LI, RHOB, X, Y, Z, MD, DTs, and NPHI. Evaluation of the models is assessed using the statistical criteria, such as the coefficient of determination (R^2), root-mean-square error (RMSE), and standard deviation (SD). First, the geomechanical parameters such as Poisson ratio, Young's modulus, and UCS are predicted using the GA–MLP algorithm, and their diagram is shown in Fig. 12. The results of R^2 between measured and predicted geomechanical properties using the GA–MLP of datasets F1–F11 are presented in Table 8.

Second, the geomechanical properties of F1–F11 are predicted using the GA–RBF model and their diagrams are indicated in Fig. 13. The results of R^2 between measured and predicted GM properties using the GA–RBF of datasets F1–F11 are given in Table 9.

The other statistical criteria applied to assess the performance of systems is the amount of RMSE error. The RMSE error quantities of geomechanical properties between the measured and predicted values have been calculated using the GA–MLP and GA–RBF methods for datasets F1–F11, and their results are presented in Tables 8 and 9.

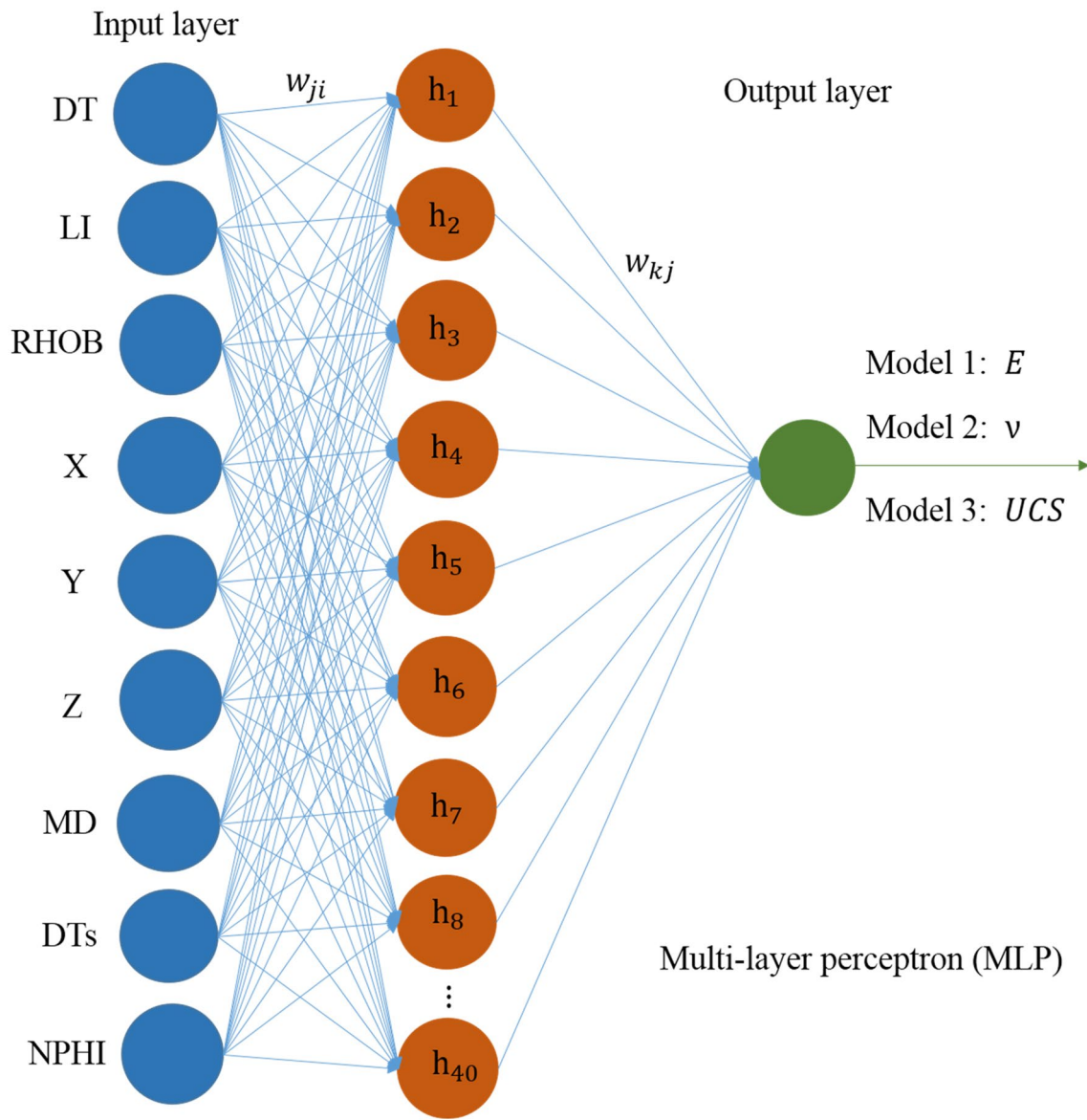


Fig. 10 Schematic of the different steps of MLP model

Table 7 Control parameter values for the GA–RBF algorithm

RBF		GA	
Control parameter	Value/options	Control parameter	Value/options
Number of inputs	9	Population	60
Number of spreads	4	Selection method	Roulette wheel
Number of input layer neurons	800	Crossover	Uniform, ($p = 1$)
Number of output layer neurons	1	Mutation	Uniform, ($p = 0.05$)
		Mutation rate	0.11
		Selection pressure for roulette wheel	2

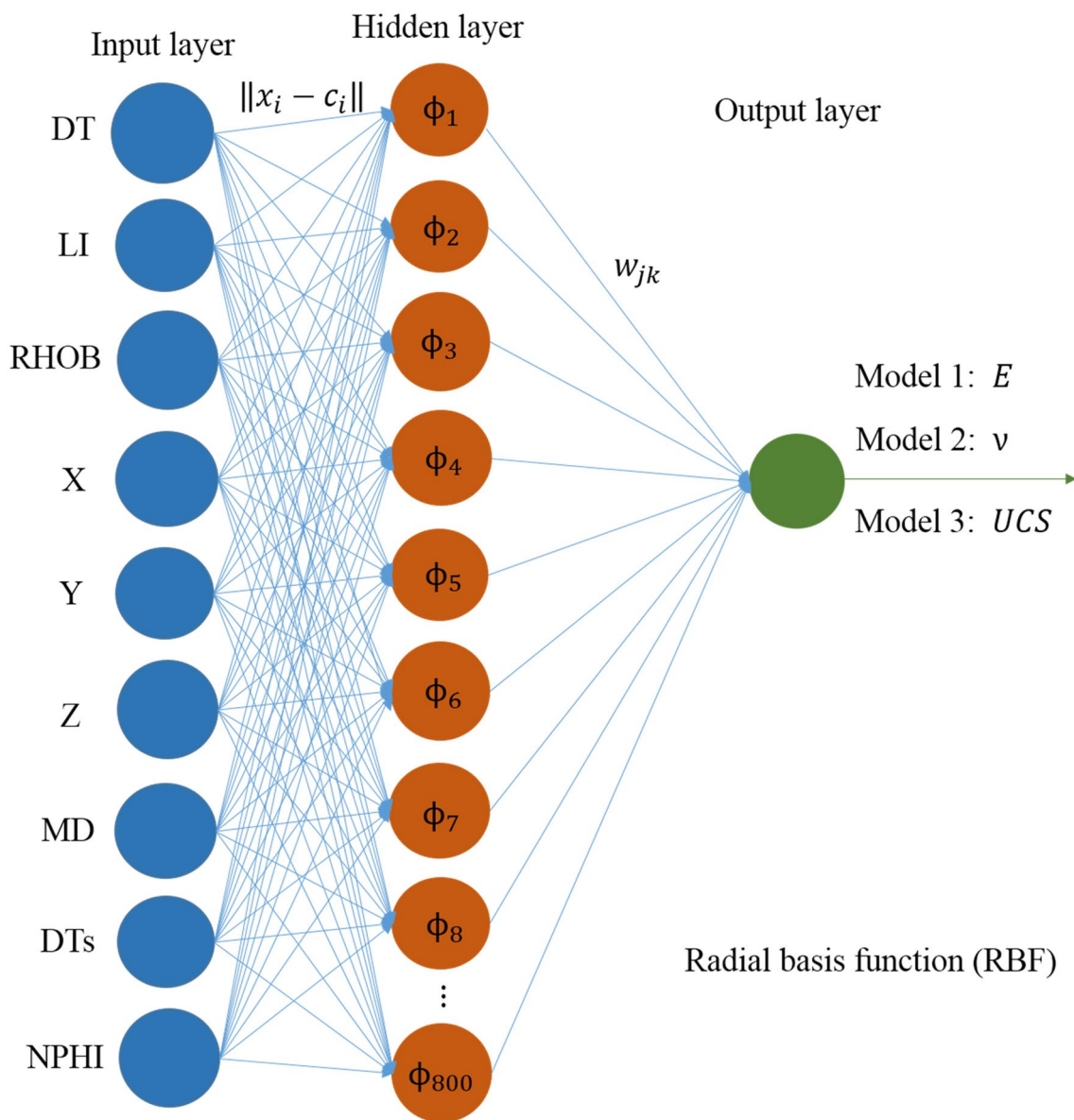


Fig. 11 Schematic of the different steps of RBF model

To compare the efficiency of GA–MLP and GA–RBF models for predicting the geomechanical properties, the coefficient of determination (R^2), RMSE error value, and standard deviation have been used. As we know, the model has acceptable performance when the value of R^2 has the highest value and close to 1 and the error values at the lowest value, i.e., close to zero.

According to the results obtained for the coefficient of determination and RMSE values given in Tables 8 and 9, the efficiency of the model has been proved. To present the accuracy of estimation, the results of the measured (targets) and estimated (outputs) geomechanical properties obtained based on the GA–MLP and GA–RBF for F1–F11 are compared and shown in Fig. 14.

According to the results of R^2 and RMSE presented in Tables 8 and 9 for estimating geomechanical properties, they are presented that the GA–MLP forecasting system has a higher performance than the GA–RBF method.

Prediction of geomechanical properties for all wells

To present the ability of MLP and RBF models to predict geomechanical properties, all data from nine wells are selected. Then, the geomechanical parameters such as including static Poisson ratio, Young’s modulus, and UCS are predicted using the GA–MLP and GA–RBF models as the same procedure described for estimating

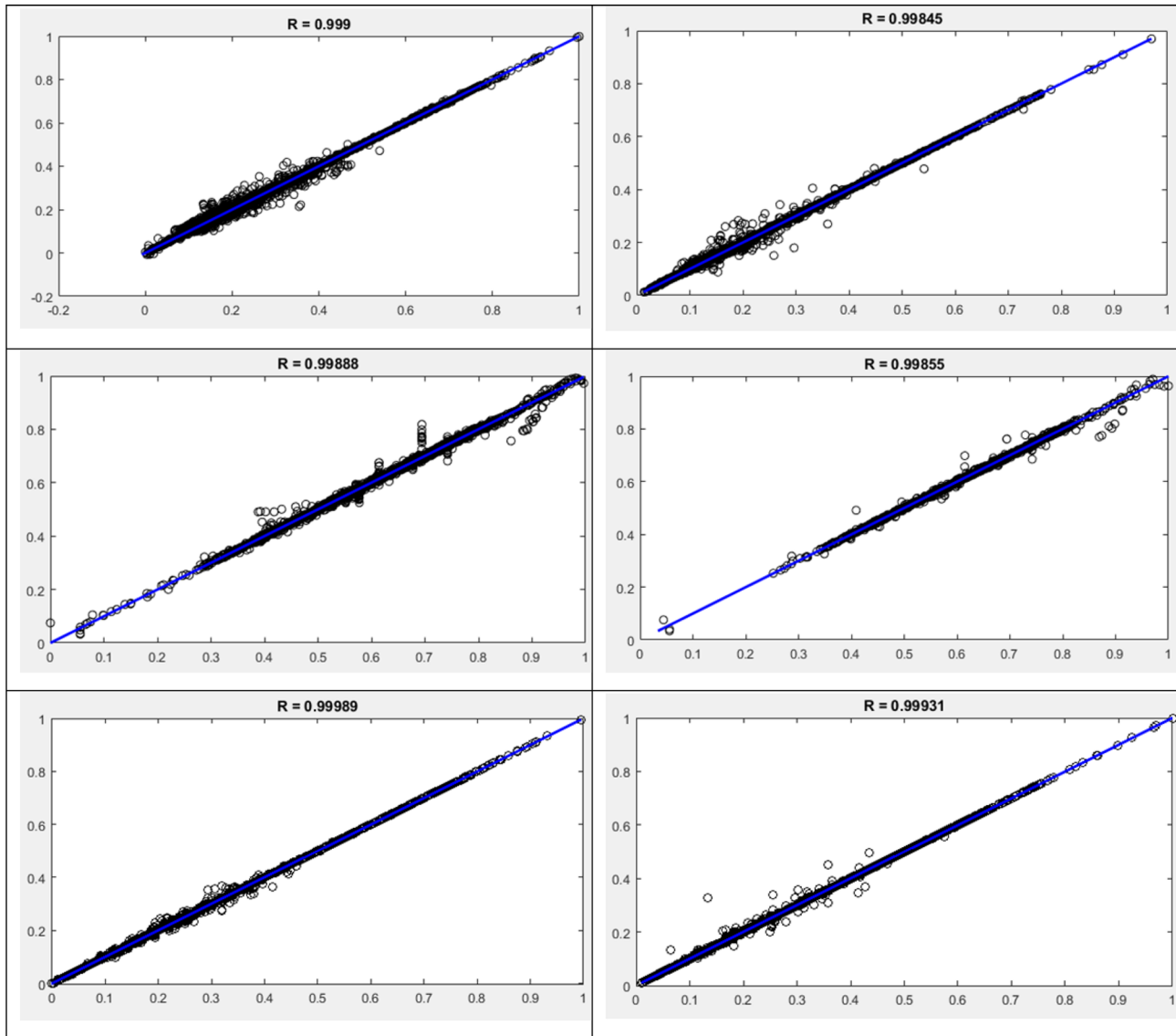


Fig. 12 The results of R^2 between measured and predicted for the datasets of F1–F11 using the GA–MLP algorithm: (top-left) static Young’s modulus for train data, (top-right) static Young’s modulus for test data, (middle-left) Poisson ratio for train data, (middle-right) Poisson ratio for test data, (bottom-left) UCS for train data, (bottom-right) UCS for test data

Table 8 Prediction of each parameter using the GA–MLP model for datasets F1–F11

Predicated parameter name	R^2			RMSE			SD		
	Train	Test	Validation	Train	Test	Validation	Train	Test	Validation
Young’s modulus	0.998	0.996	0.996	0.0061	0.0073	0.0079	0.0061	0.0073	0.0079
Poisson ratio	0.997	0.997	0.996	0.0043	0.0050	0.0055	0.0043	0.0050	0.0055
UCS	0.999	0.998	0.999	0.0019	0.0049	0.0032	0.0019	0.0049	0.0032

the geomechanical properties of datasets F1–F11. The results of R^2 , RMSE, and SD by using the GA–MLP and GA–RBF models for data from nine wells are presented in Table 10. In addition, to show the accuracy of estimation,

the results of the measured and estimated geomechanical properties obtained from all nine well data are compared and given in Fig. 15.

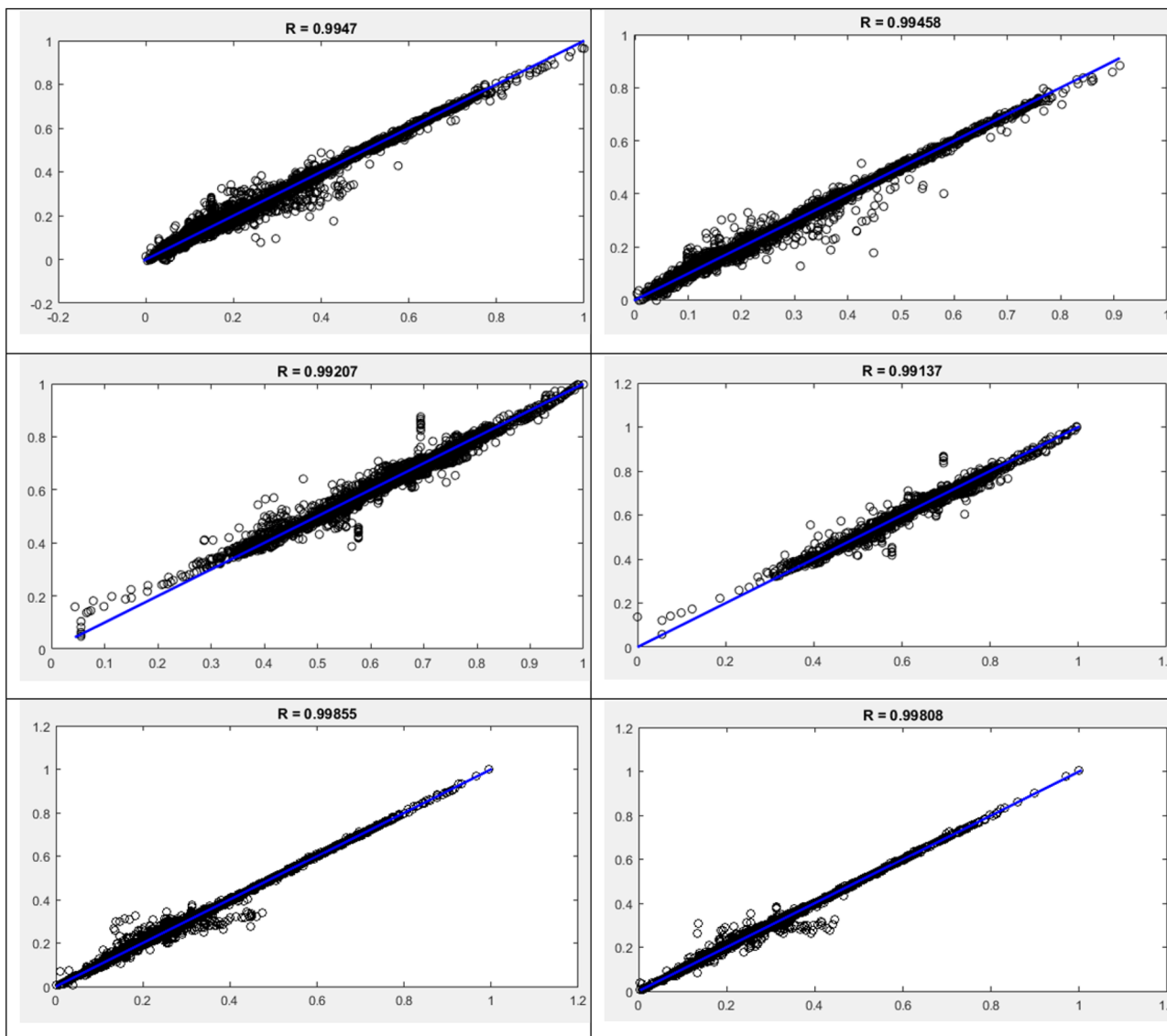


Fig. 13 The results of R^2 between measured and predicted for the datasets of F1–F11 using the GA–RBF algorithm: (top-left) static Young’s modulus for train data, (top-right) static Young’s modulus

for test data, (middle-left) Poisson ratio for train data, (middle-right) Poisson ratio for test data, (bottom-left) UCS for train data, (bottom-right) UCS for test data

Table 9 Prediction of each parameter using the GA–RBF model for datasets F1–F11

Predicated parameter name	R^2			RMSE			SD		
	Train	Test	Validation	Train	Test	Validation	Train	Test	Validation
Young’s modulus	0.989	0.989	0.989	0.0138	0.0140	0.0144	0.0138	0.014	0.0144
Poisson ratio	0.984	0.982	0.981	0.0116	0.0121	0.0125	0.0116	0.0121	0.0125
UCS	0.997	0.996	0.997	0.0071	0.0081	0.0076	0.0071	0.0081	0.0076

According to the results of R^2 and RMSE presented in Table 10 for estimating geomechanical properties, they are

shown that the GA–MLP forecasting system has a higher performance than the GA–RBF method.

Since this paper uses a large number of datasets for ML methods, the results show that the ML methods in this study

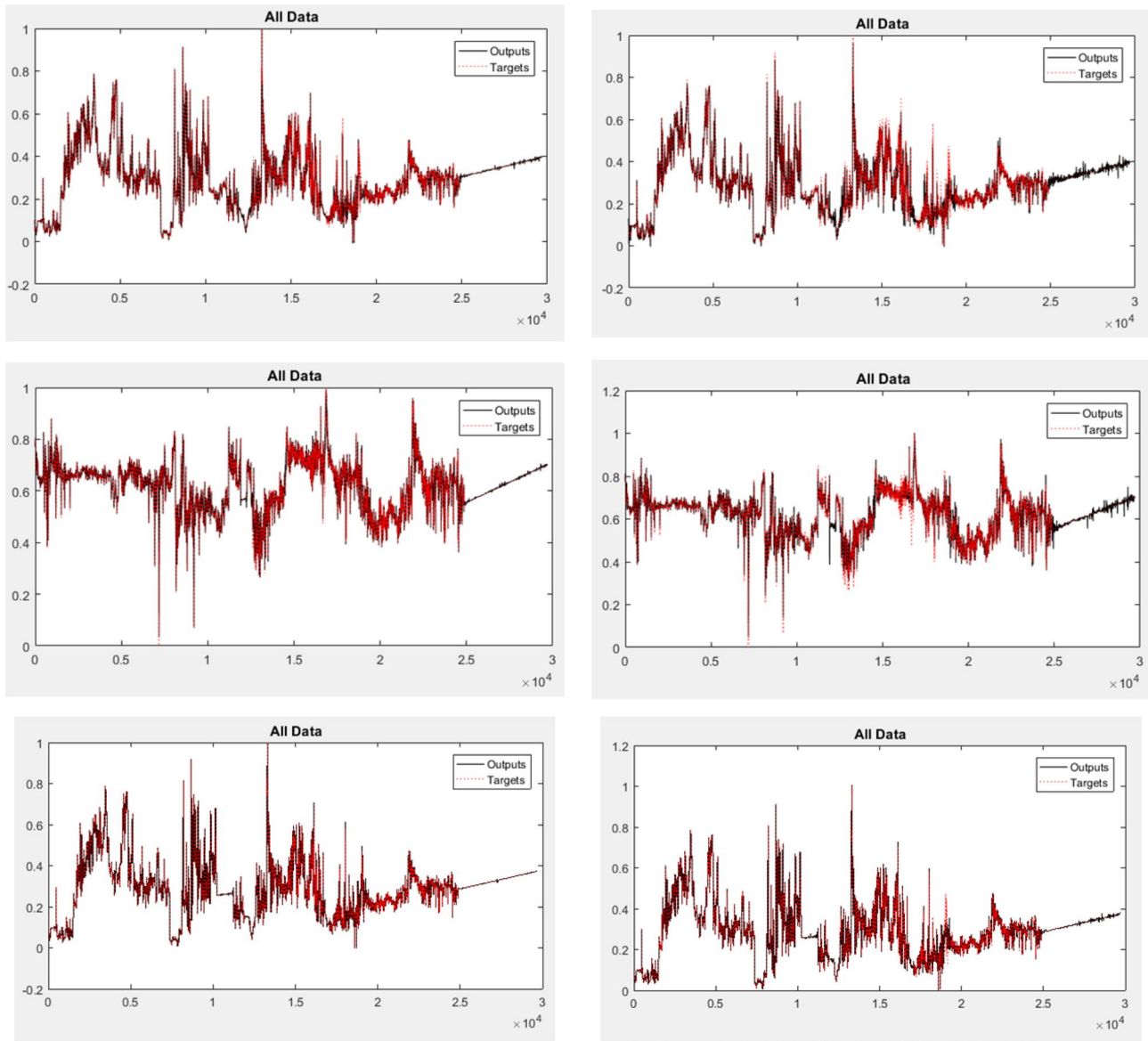


Fig. 14 The comparison between measured (targets) and estimated (outputs) values of: (top-left) static Young’s modulus based on the GA–MLP algorithm, (top-right) static Young’s modulus based on the GA–RBF algorithm, (middle-left) Poisson ratio based on the GA–

MLP algorithm, (middle-right) Poisson ratio based on the GA–RBF algorithm, (bottom-left) UCS based on the GA–MLP algorithm, (bottom-right) UCS based on the GA–RBF algorithm

Table 10 Prediction of static Young’s modulus using the GA–MLP and GA–RBF models for all wells

Name of parameter	Predictive model	R ²			RMSE			SD		
		Train	Test	Validation	Train	Test	Validation	Train	Test	Validation
Static Young’s modulus	GA–MLP	0.964	0.964	0.962	0.0291	0.0291	0.0298	0.0291	0.0291	0.0298
Static Young’s modulus	GA–RBF	0.905	0.904	0.903	0.0471	0.0478	0.0481	0.0471	0.0478	0.0481
Poisson ratio	GA–MLP	0.783	0.768	0.792	0.0565	0.0586	0.0555	0.0565	0.0586	0.0555
Poisson ratio	GA–RBF	0.548	0.539	0.542	0.0815	0.0827	0.0816	0.0815	0.0828	0.0816
UCS	GA–MLP	0.998	0.998	0.998	0.0034	0.0039	0.0034	0.0034	0.0039	0.0034
UCS	GA–RBF	0.995	0.995	0.0065	0.0067	0.0065	0.0065	0.0067	0.0065	0.995

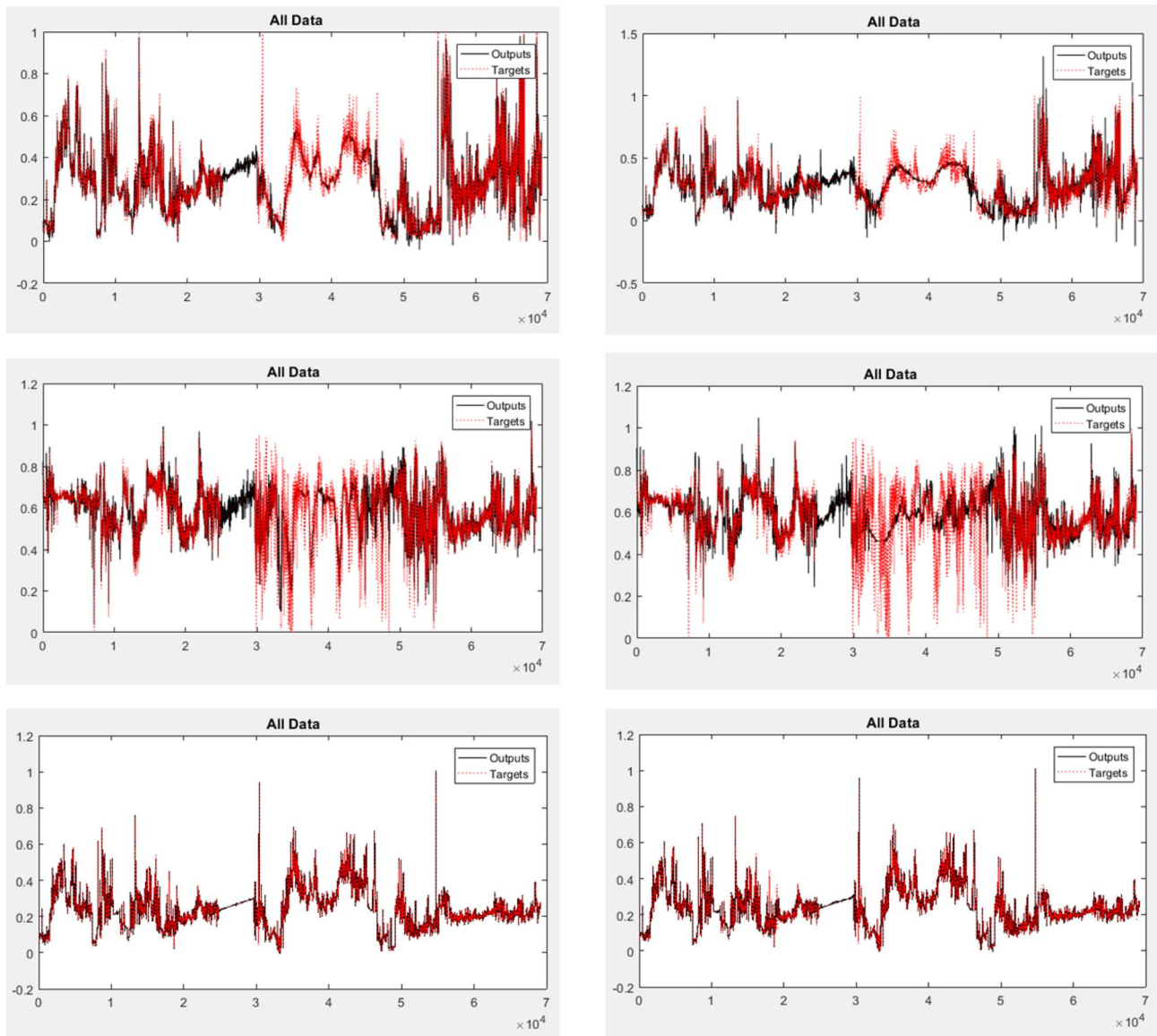


Fig. 15 The comparison between measured (targets) and estimated (outputs) values of: (top-left) static Young's modulus based on the GA-MLP algorithm, (top-right) static Young's modulus based on the GA-RBF algorithm, (middle-left) Poisson ratio based on the GA-

MLP algorithm, (middle-right) Poisson ratio based on the GA-RBF algorithm, (bottom-left) UCS based on the GA-MLP algorithm, (bottom-right) UCS based on the GA-RBF algorithm

can be used for other datasets by reducing or increasing the number of data, and the methods still have the same results.

At the end of this section, to guide other researchers who intend to estimate GM parameters, it can be stated that the anisotropy of the reservoir rock must be taken into account when estimating GM parameters using ML methods. Because at the same time, there is a wide range of continuous well-logging data and limited geomechanical laboratory data. This problem makes the estimation of GM parameters based on well-logging data a little difficult. However, the results of this research show that the

most appropriate method for continuous estimation of GM parameters is estimated based on ML methods.

Thus, one of the proposals to estimate GM parameters, which is a very complex task without uncertainty, is the development of software in this direction based on ML methods. However, it is necessary that before using the methods developed in the software, laboratory data must be measured using suitable apparatus on the rock core at the desired depth so that this information can be used to validate the results.

Conclusions

In this study, a robust machine learning (ML) model to compute geomechanical (GM) parameters from the complex dataset was proposed. To propose the model, the following remarks were made:

1. The large data sets of the Volve oil field were used to predict the GM parameters using two recombinant algorithms of ML methods: genetic algorithm (GA)–multi-layer perceptron (MLP) and genetic algorithm (GA)–radial basis function (RBF).
2. The feature selection was used to avoid unessential inputs to achieve the best results.
3. MLP and RBF algorithms were optimized using GA optimizers. The GA–MLP and GA–RBF models were considered in one step followed by another to calculate the number of hidden layers and neurons in order to finally identify the optimal weights and biases for the ML methods. This process led to combining GA with MLP and RBF to predict accurately the GM parameters.
4. The comparison of GA–MLP and GA–RBF models indicated that the GA–MLP has higher performance accuracy to predict GM parameters.
5. The proposed method provides insights for applying ML methods to improve accuracy in order to generate the best performance for the prediction of the GM parameters.
6. The results showed that the proposed ML models in this study still have the same results for another unseen dataset.

Funding All authors certify that they have no affiliations with or involvement in any organization or entity with any financial interest or non-financial interest in the subject matter or materials discussed in this manuscript.

Declarations

Conflict of interest The authors have no conflicts of interest to declare that are relevant to the content of this article.

Open Access This article is licensed under a Creative Commons Attribution 4.0 International License, which permits use, sharing, adaptation, distribution and reproduction in any medium or format, as long as you give appropriate credit to the original author(s) and the source, provide a link to the Creative Commons licence, and indicate if changes were made. The images or other third party material in this article are included in the article's Creative Commons licence, unless indicated otherwise in a credit line to the material. If material is not included in the article's Creative Commons licence and your intended use is not permitted by statutory regulation or exceeds the permitted use, you will need to obtain permission directly from the copyright holder. To view a copy of this licence, visit <http://creativecommons.org/licenses/by/4.0/>.

References

- Abdulraheem A, Ahmed M, Vantala A, Parvez T (2009) Prediction of rock mechanical parameters for hydrocarbon reservoirs using different artificial intelligence techniques. In: Presented at the SPE Saudi Arabia section technical symposium. <https://doi.org/10.2118/126094-ms>
- Ahmadi M, Chen Z (2020) Machine learning-based models for predicting permeability impairment due to scale deposition. *J Petrol Explor Prod Technol* 10(7):2873–2884. <https://doi.org/10.1007/s13202-020-00941-1>
- Ahmed A, Elkhatny S, Alsaihati A (2021) Applications of artificial intelligence for static Poisson's ratio prediction while drilling. *Comput Intell Neurosci* 2021:1–10. <https://doi.org/10.1155/2021/9956128>
- Afsari M, Ghafoori MR, Roostaieian M, Haghshenas A, Ataei A, Masoudi R (2009) Mechanical earth model (MEM): an effective tool for borehole stability analysis and managed pressure drilling (case study). In: All Days. SPE middle east oil and gas show and conference. SPE. <https://doi.org/10.2118/118780-ms>
- Aghakhani Emamqeyasi MR, Fatehi Marji M, Hashemizadeh A, Abdollahipour A, Sanei M (2023) Prediction of elastic parameters in gas reservoirs using ensemble approach. *Environ Earth Sci*. <https://doi.org/10.1007/s12665-023-10958-4>
- Ahmed A, Mahmoud AA, Elkhatny S (2019) Fracture pressure prediction using radial basisfunction. In: AAE National technical conference and exhibition, AAE-19-NTCE-061, Denver, CO. https://www.aade.org/application/files/1415/7132/0393/AAE-19-NTCE-061_-_Ahmed_S.pdf
- Aladejare AE (2016) Development of Bayesian probabilistic approaches for rock property characterization. Doctoral dissertation, City University of Hong Kong
- Aladejare AE (2020) Evaluation of empirical estimation of uniaxial compressive strength of rock using measurements from index and physical tests. *J Rock Mech Geotech Eng* 12(2):256–268. <https://doi.org/10.1016/j.jrmge.2019.08.001>
- Al-Anazi BD, Al-Garni MT, Muffareh T, Al-Mushigeh I (2011) Prediction of Poisson's ratio and Young's modulus for hydrocarbon reservoirs using alternating conditional expectation algorithm. In: All Days. SPE middle east oil and gas show and conference. SPE. <https://doi.org/10.2118/138841-ms>
- Aliouane L, Ouadfeul SA, Boudella A (2015) Pore pressure prediction in shale gas reservoirs using neural network and fuzzy logic with an application to Barnett Shale. In: EGU General Assembly Conference. Vienna, Austria
- Ali J (1994) Neural networks: a new tool for the petroleum industry? SPE-27561-MS. In: European petroleum computer conference society of petroleum engineers. <https://doi.org/10.2118/27561-ms>
- Anysz H, Zbiciak A, Ibadov N (2016) The influence of input data standardization method on prediction accuracy of artificial neural networks. *Procedia Eng* 153:66–70. <https://doi.org/10.1016/j.proeng.2016.08.081>
- Archer S, Rasouli V (2012) A log based analysis to estimate mechanical properties and in-situ stresses in a shale gas well in North Perth Basin. *Pet Min Res*. <https://doi.org/10.2495/pmr120151>
- Armaghani DJ, Mohamad ET, Momeni E, Narayanasamy MS, Mohd Amin MF (2015) An adaptive neuro-fuzzy inference system for predicting unconfined compressive strength and Young's modulus: a study on main range granite. *Bull Eng Geol Environ* 74(4):1301–1319. <https://doi.org/10.1007/s10064-014-0687-4>
- Asadi A (2017) Application of artificial neural networks in prediction of uniaxial compressive strength of rocks using well logs and drilling data. *Procedia Eng* 191:279–286. <https://doi.org/10.1016/j.proeng.2017.05.182>

- Asoodeh M (2013) Prediction of Poisson's ratio from conventional well log data: a committee machine with intelligent systems approach. *Energy Sources Part A Recovery Util Environ Effects* 35(10):962–975. <https://doi.org/10.1080/15567036.2011.557693>
- Bansal P, Lamba R, Jain V, Jain T, Shokeen S, Kumar S, Singh PK, Khan BGGA-MLP (2022) A greedy genetic algorithm to optimize weights and biases in multilayer perceptron. *Contrast Media Mol Imaging* 24:4036035. <https://doi.org/10.1155/2022/4036035>
- Bradford IDR, Fuller J, Thompson PJ, Walsgrove TR (1998) Benefits of assessing the solids production risk in a North Sea reservoir using elastoplastic modelling. In *All Days. SPE/ISRM rock mechanics in petroleum engineering*. SPE. <https://doi.org/10.2118/47360-ms>
- Chang C, Zoback MD, Khaksar A (2006) Empirical relations between rock strength and physical properties in sedimentary rocks. *J Pet Sci Eng* 51(3–4):223–237. <https://doi.org/10.1016/j.petrol.2006.01.003>
- Costa LAN, Maschio C, José Schiozer D (2014) Application of artificial neural networks in a history matching process. *J Pet Sci Eng* 123:30–45. <https://doi.org/10.1016/j.petrol.2014.06.004>
- Doraisamy H, Ertekin T, Grader AS (1998) Key parameters controlling the performance of neuro-simulation applications in field development. In *All Days. SPE eastern regional meeting*, pp 233–241. <https://doi.org/10.2118/51079-ms>
- Delavar MR, Ramezanzadeh A, Gholami R, Sanei M (2023) Optimization of drilling parameters using combined multi-objective method and presenting a practical factor. *Comput Geosci*. <https://doi.org/10.1016/j.cageo.2023.105359>
- Elkatatny S, Mahmoud M (2018) Development of new correlations for the oil formation volume factor in oil reservoirs using artificial intelligent white box technique. *Petroleum* 4(2):178–186. <https://doi.org/10.1016/j.petlm.2017.09.009>
- Elkatatny S, Tariq Z, Mahmoud M, Abdulraheem A, Mohamed I (2019) An integrated approach for estimating static Young's modulus using artificial intelligence tools. *Neural Comput Appl* 31(8):4123–4135. <https://doi.org/10.1007/s00521-018-3344-1>
- Elsafi SH (2014) Artificial neural networks (ANNs) for flood forecasting at Dongola station in the River Nile, Sudan. *Alex Eng J* 53(3):655–662. <https://doi.org/10.1016/j.aej.2014.06.010>
- Equinor Website Database (2021) Available online: <https://www.equinor.com/en/how-and-why/digitalisation-in-our-dna/olve-field-data-village-download.html>. Accessed 9 July 2021
- Fatehi M, Asadi HH (2017) Data integration modeling applied to drill hole planning through semi-supervised learning: a case study from the Dalli Cu–Au porphyry deposit in the central Iran. *J Afr Earth Sci* 128:147–160. <https://doi.org/10.1016/j.jafrearsci.2016.09.007>
- Fjær E, Holt R, Horsrud P, Raaen A (2008) *Petroleum related rock mechanics*. Elsevier Science, Amsterdam
- Gholami R, Moradzadeh A, Rasouli V, Hanachi J (2014) Practical application of failure criteria in determining safe mud weight windows in drilling operations. *J Rock Mech Geotech Eng* 6(1):13–25. <https://doi.org/10.1016/j.jrmge.2013.11.002>
- Gong A, Zhang Y, Sun Y, Lin W, Wang J (2023) A nuclear magnetic resonance proxy model for predicting movable fluid of rocks based on adaptive ensemble learning. *Phys Fluids* 35(3):033106. <https://doi.org/10.1063/5.0140372>
- Gowida A, Elkatatny S, Gamal H (2020) Unconfined compressive strength (UCS) prediction in real-time while drilling using artificial intelligence tools. *Neural Comput Appl*. <https://doi.org/10.1007/s00521-020-05546-7>
- Gu Y, Bao Z, Cui G (2018) Permeability prediction using hybrid techniques of continuous restricted Boltzmann machine, particle swarm optimization and support vector regression. *J Nat Gas Sci Eng* 59:97–115. <https://doi.org/10.1016/j.jngse.2018.08.020>
- Güllü H, Jaf HS (2016) Full 3D nonlinear time history analysis of dynamic soil–structure interaction for a historical masonry arch bridge. *Environ Earth Sci* 75:1421. <https://doi.org/10.1007/s12665-016-6230-0>
- Güllü H, Pala M (2014) On the resonance effect by dynamic soil–structure interaction: a revelation study. *Nat Hazards* 72:827–847. <https://doi.org/10.1007/s11069-014-1039-1>
- Ham F, Kostanic I (2001) *Fundamental neurocomputing concepts. Principles of neurocomputing for science and engineering*. Arnold Publishers, London
- Hareland G, Nygård R (2007) Calculating unconfined rock strength from drilling data. In: *1st Canada–U.S. rock mechanics symposium, Vancouver, British Columbia, Canada. ARMA-07-214*
- Hassanvand M, Moradi S, Fattahi M, Zargar G, Kamari M (2018) Estimation of rock uniaxial compressive strength for an Iranian carbonate oil reservoir: modeling vs. artificial neural network application. *Pet Res* 3(4):336–345. <https://doi.org/10.1016/j.ptlrs.2018.08.004>
- Haykin S (1999) *Neural networks: a comprehensive foundation*, 2nd edn. Prentice Hall International, New Jersey
- He M, Zhang Z, Ren J, Huan J, Li G, Chen Y, Li N (2019) Deep convolutional neural network for fast determination of the rock strength parameters using drilling data. *Int J Rock Mech Min Sci* 123:104084. <https://doi.org/10.1016/j.ijrmm.2019.104084>
- Holland JH (1992) *Adaptation in natural and artificial systems: an introductory analysis with applications to biology, control and artificial intelligence*. MIT Press, Cambridge
- Hornik K (1991) Approximation capabilities of multilayer feedforward networks. *Neural Netw* 4(2):251–257. [https://doi.org/10.1016/0893-6080\(91\)90009-t](https://doi.org/10.1016/0893-6080(91)90009-t)
- Ibrahim AF, Gowida A, Ali A, Elkatatny S (2021) Machine learning application to predict in-situ stresses from logging data. *Sci Rep* 11(1):23445. <https://doi.org/10.1038/s41598-021-02959-9>
- Jamshidi E, Arabjamaloei R, Hashemi A, Ekramzadeh MA, Amani M (2013) Real-time estimation of elastic properties of formation rocks based on drilling data by using an artificial neural network. *Energy Sources Part A Recovery Util Environ Effects* 35(4):337–351. <https://doi.org/10.1080/15567036.2010.495971>
- Jia W, Zhao D, Shen T, Su C, Hu C, Zhao Y (2014) A new optimized GA–RBF neural network algorithm. *Comput Intell Neurosci* 2014:1–6. <https://doi.org/10.1155/2014/982045>
- Jin Z, He D, Ma R, Zou X, Chen Y, Shan S (2022) Fault diagnosis of train rotating parts based on multi-objective VMD optimization and ensemble learning. *Digit Signal Process* 121:103312. <https://doi.org/10.1016/j.dsp.2021.103312>
- Khatibi S, Aghajanzadeh A (2020) Machine learning: a useful tool in geomechanical studies, a case study from an offshore gas field. *Energies* 13(14):3528. <https://doi.org/10.3390/en13143528>
- Kubota L, Reinert D (2019) Machine learning forecasts oil rate in mature onshore field jointly driven by water and steam injection. In: *Day 2 Tue, October 01, 2019. In: SPE annual technical conference and exhibition. SPE*. <https://doi.org/10.2118/196152-ms>
- Lacy LL (1997) Dynamic rock mechanics testing for optimized fracture designs. In: *All Days. SPE annual technical conference and exhibition. SPE*. <https://doi.org/10.2118/38716-ms>
- Mahmoud A, Elkatatny S, Chen W, Abdulraheem A (2019a) Estimation of oil recovery factor for water drive sandy reservoirs through applications of artificial intelligence. *Energies* 12(19):3671. <https://doi.org/10.3390/en12193671>
- Mahmoud AA, Elkatatny S, Ali A, Moussa T (2019b) Estimation of static Young's modulus for sandstone formation using artificial neural networks. *Energies* 12(11):2125. <https://doi.org/10.3390/en12112125>
- Mahmoud AA, Elkatatny S, Al Shehri D (2020) Application of machine learning in evaluation of the static Young's modulus for

- sandstone formations. *Sustainability* 12(5):1880. <https://doi.org/10.3390/su12051880>
- Mavko G, Mukerji T, Dvorkin J (2020) *The rock physics handbook*. Cambridge University Press, Cambridge
- Menzies T, Kocaguneli E, Turhan B, Minku L, Peters F (2014) *Sharing data and models in software engineering*. Morgan Kaufmann Publishers Inc., San Francisco, CA, USA
- Mohaghegh S (2000) Virtual-intelligence applications in petroleum engineering: part 1-artificial neural networks. *J Pet Technol* 52(09):64–73. <https://doi.org/10.2118/58046-jpt>
- Nabaei M, Shahbazian K (2012) A new approach for predrilling the unconfined rock compressive strength prediction. *Pet Sci Technol* 30(4):350–359. <https://doi.org/10.1080/10916461003752546>
- Naeni EZ, Green S, Russell-Hughes I, Rauch-Davies M (2019) An integrated deep learning solution for petrophysics, pore pressure, and geomechanics property prediction. *Lead Edge* 38(1):53–59. <https://doi.org/10.1190/tle38010053.1>
- Najibi AR, Ghafoori M, Lashkaripour GR, Asef MR (2015) Empirical relations between strength and static and dynamic elastic properties of Asmari and Sarvak limestones, two main oil reservoirs in Iran. *J Pet Sci Eng* 126:78–82. <https://doi.org/10.1016/j.petrol.2014.12.010>
- Okpo EE, Dosunmu A, Odagme BS (2016) Artificial neural network model for predicting wellbore instability. In: All Days. SPE Nigeria annual international conference and exhibition. SPE. <https://doi.org/10.2118/184371-ms>
- Plona TJ, Cook JM (1995) Effects of stress cycles on static and dynamic Young's moduli in Castlegate sandstone, *Rock Mechanics*. In: Daemen JJK, Schultz RA, BMkema (eds) *Proceedings of the 35th U.S. Symposium*. A. A. BMkema, Rotterdam, Netherlands, p 155
- Rajabi M, Beheshtian S, Davoodi S, Ghorbani H, Mohamadian N, Radwan AE, Alvar MA (2021) Novel hybrid machine learning optimizer algorithms to prediction of fracture density by petrophysical data. *J Pet Explor Prod Technol* 11(12):4375–4397. <https://doi.org/10.1007/s13202-021-01321-z>
- Rampersad, PR, Hareland G, Boonyapaluk P (1994) Drilling optimization using drilling data and available technology. In SPE Latin America/Caribbean petroleum engineering conference. Society of Petroleum Engineers. <https://doi.org/10.2118/27034-ms>
- Rashidi M, Asadi A (2018) An artificial intelligence approach in estimation of formation pore pressure by critical drilling data. In: 52nd U.S. Rock mechanics/geomechanics symposium, No. 1959. ARMA-2018–1098
- Ranjbar-Karami R, Kadkhodaie-Ilkhchi A, Shiri M (2014) A modified fuzzy inference system for estimation of the static rock elastic properties: a case study from the Kangan and Dalan gas reservoirs, South Pars gas field, the Persian Gulf. *J Nat Gas Sci Eng* 21:962–976. <https://doi.org/10.1016/j.jngse.2014.10.034>
- Rojas R (1996) *Neural Networks*. Springer, Berlin, Heidelberg
- Sachpazis CI (1990) Correlating schmidt hardness with compressive strength and young's modulus of carbonate rocks. *Bull Int Assoc Eng Geol* 42(1):75–83. <https://doi.org/10.1007/bf02592622>
- Sanei M, Faramarzi L, Goli S, Fahimifar A, Rahmati A, Mehinrad A (2013) Development of a new equation for joint roughness coefficient (JRC) with fractal dimension: a case study of Bakhtiary Dam site in Iran. *Arab J Geosci* 8(1):465–475. <https://doi.org/10.1007/s12517-013-1147-3>
- Sanei M, Faramarzi L (2014) Empirical development of the rock mass deformation modulus. *J Geol Res Eng* 2(1):55–67. <https://doi.org/10.17265/2328-2193/2014.01.006>
- Sanei M, Faramarzi L, Fahimifar A, Goli S, Mehinrad A, Rahmati A (2015) Shear strength of discontinuities in sedimentary rock masses based on direct shear tests. *Int J Rock Mech Min Sci* 75:119–131. <https://doi.org/10.1016/j.ijrmms.2014.11.009>
- Sanei M, Devloo PRB, Forti TLD, Durán O, Santos ESR (2021a) An innovative scheme to make an initial guess for iterative optimization methods to calibrate material parameters of strain-hardening elastoplastic models. *Rock Mech Rock Eng* 55(1):399–421. <https://doi.org/10.1007/s00603-021-02665-y>
- Sanei M, Durán O, Devloo PRB, Santos ESR (2021b) Analysis of pore collapse and shear-enhanced compaction in hydrocarbon reservoirs using coupled poro-elastoplasticity and permeability. *Arab J Geosci*. <https://doi.org/10.1007/s12517-021-06754-8>
- Sanei M, Durán O, Devloo PRB, Santos ESR (2022) Evaluation of the impact of strain-dependent permeability on reservoir productivity using iterative coupled reservoir geomechanical modeling. *Geomech Geophy Geo Energy Geo Res*. <https://doi.org/10.1007/s40948-022-00344-y>
- Sen S, Ganguli SS (2019) Estimation of pore pressure and fracture gradient in Volve Field, Norwegian North Sea. In: Day 2 Wed, April 10, 2019. SPE Oil and Gas India Conference and Exhibition. SPE. <https://doi.org/10.2118/194578-ms>
- Siddig O, Elkatatny S (2021) Workflow to build a continuous static elastic moduli profile from the drilling data using artificial intelligence techniques. *J Pet Explor Prod Technol* 11(10):3713–3722. <https://doi.org/10.1007/s13202-021-01274-3>
- Siddig O, Gamal H, Elkatatny S, Abdurraheem A (2021) Real-time prediction of Poisson's ratio from drilling parameters using machine learning tools. *Sci Rep* 11(1):12611. <https://doi.org/10.1038/s41598-021-92082-6>
- Schlumberger (2018) *Techlog wellbore stability analysis workflow/ solutions training*
- Szydluk TJ, Way S, Smith P, Aamodt L, Friedrich C (2006) 3D PP/PS prestack depth migration on the Volve Field. In: 68th EAGE conference and exhibition incorporating SPE EUROPEC 2006. European Association of Geoscientists and Engineers. <https://doi.org/10.3997/2214-4609.201402177>
- Tariq Z, Elkatatny S, Mahmoud M, Ali AZ, Abdurraheem A (2017a) A new approach to predict failure parameters of carbonate rocks using artificial intelligence tools. In: Day 4 Thu, April 27, 2017a. SPE Kingdom of Saudi Arabia annual technical symposium and exhibition. SPE, pp 1428–1440. <https://doi.org/10.2118/187974-ms>
- Tariq Z, Elkatatny S, Mahmoud MA, Abdurraheem A, Abdelwahab AZ, Woldeamanuel M (2017b) Estimation of rock mechanical parameters using artificial intelligence tools. In: 51st U.S. Rock Mech Symp 11. Paper Number: ARMA-2017b-0301
- Tariq Z, Mahmoud M, Abdurraheem A (2019) An artificial intelligence approach to predict the water saturation in carbonate reservoir rocks. In Day 2 Tue, October 01, 2019. SPE annual technical conference and exhibition. SPE. <https://doi.org/10.2118/195804-ms>
- Tiab D, Donaldson EC (2015) *Petrophysics: theory and practice of measuring reservoir rock and fluid transport properties*. Gulf professional publishing, Houston
- Ulusay R, Tureli K, Ider MH (1994) Prediction of engineering properties of a selected litharenite sandstone from its petrographic characteristics using correlation and multivariate statistical techniques. *Eng Geol* 38(1–2):135–157. [https://doi.org/10.1016/0013-7952\(94\)90029-9](https://doi.org/10.1016/0013-7952(94)90029-9)
- Wang HF (2000) *Theory of linear poroelasticity*. Princeton University Press, Princeton
- Wang B, Sharma J, Chen J, Persaud P (2021) Ensemble machine learning assisted reservoir characterization using field production data—an offshore field case study. *Energies* 14(4):1052. <https://doi.org/10.3390/en14041052>
- Wei L, Cheng Z, Cheng J, Hu N, Yang Y (2022) A fault detection method based on an oiltemperature forecasting model using an improved deep deterministic policy gradient algorithm in the helicopter gearbox. *Entropy* 24(10):1394. <https://doi.org/10.3390/e24101394>

- Xu H, Zhou W, Xie R, Da L, Xiao C, Shan Y, Zhang H (2016) Characterization of rock mechanical properties using lab tests and numerical interpretation model of well logs. *Mathe Probl Eng* 2016:1–13. <https://doi.org/10.1155/2016/5967159>
- Yu B, He X (2006) Training radial basis function networks with differential evolution. In: *IEEE international conference on granular computing, GrC 2006*. Atlanta, Georgia, USA, pp 369–372. <https://doi.org/10.1109/GRC.2006.1635817>
- Zhang JJ, Bentley LR (2005) Factors determining Poisson's ratio. *CREWES Res Rep* 17:1–15
- Zhang JJ (2020) *Applied petroleum geomechanics*. Gulf Professional Publishing, Houston
- Zhao B, Ratnakar R, Dindoruk B, Mohanty K (2020) A hybrid approach for the prediction of relative permeability using machine learning of experimental and numerical proxy SCAL data. *SPE J* 25(05):2749–2764. <https://doi.org/10.2118/196022-pa>
- Zoback MD (2010) *Reservoir geomechanics*. Cambridge University Press, Cambridge

Publisher's Note Springer Nature remains neutral with regard to jurisdictional claims in published maps and institutional affiliations.